



HAL
open science

Suspended sediment properties in the Lower Mekong River, from fluvial to estuarine environments

Hoang-Anh Le, Nicolas Gratiot, William Santini, Olivier Ribolzi, Duc Tran, Xavier Meriaux, Eric Deleersnijder, Sandra Soares-Frazaõ

► **To cite this version:**

Hoang-Anh Le, Nicolas Gratiot, William Santini, Olivier Ribolzi, Duc Tran, et al.. Suspended sediment properties in the Lower Mekong River, from fluvial to estuarine environments. *Estuarine, Coastal and Shelf Science*, 2020, 233, pp.106522. 10.1016/j.ecss.2019.106522 . hal-03489755

HAL Id: hal-03489755

<https://hal.science/hal-03489755>

Submitted on 21 Jul 2022

HAL is a multi-disciplinary open access archive for the deposit and dissemination of scientific research documents, whether they are published or not. The documents may come from teaching and research institutions in France or abroad, or from public or private research centers.

L'archive ouverte pluridisciplinaire **HAL**, est destinée au dépôt et à la diffusion de documents scientifiques de niveau recherche, publiés ou non, émanant des établissements d'enseignement et de recherche français ou étrangers, des laboratoires publics ou privés.



Distributed under a Creative Commons Attribution - NonCommercial 4.0 International License

1 **Suspended sediment properties in the Lower Mekong River, from fluvial to** 2 **estuarine environments**

3

4 **Hoang-Anh Le**^{1,2}, **Nicolas Gratiot**^{2,3,*}, **William Santini**⁴, **Olivier Ribolzi**⁴, **Duc Tran**⁵,
5 **Xavier Meriaux**⁶, and **Eric Deleersnijder**^{7,8}, **Sandra Soares-Frazaõ**¹

6

7 ¹ Civil and Environmental Engineering, Institute of Mechanics, Materials and Civil Engineering (IMMC),
8 Université catholique de Louvain, Place du Levant 1, B-1348 Louvain – la – Neuve, Belgium

9 ² Asian Research Center on Water (CARE-Rescif), Ho Chi Minh City University of Technology, Block B7, 268
10 Ly Thuong Kiet Street, District 10, Ho Chi Minh City, Vietnam

11 ³ CNRS, IRD, IGE, Université Grenoble Alpes, F-38000 Grenoble, France

12 ⁴ Géosciences Environnement Toulouse (GET), Université de Toulouse, IRD, CNRS, UPS, Toulouse, France

13 ⁵ Faculty of Environment and Natural Resources, Ho Chi Minh City University of Technology, VNU-HCM,
14 268 Ly Thuong Kiet, Ho Chi Minh City, Vietnam

15 ⁶ Université Littoral Côte d’Opale, Université Lille, CNRS, UMR 8187, LOG, Laboratoire d’Océanologie et de
16 Géosciences, F 62930Wimereux, France

17 ⁷ Université catholique de Louvain, Institute of Mechanics, Materials and Civil Engineering (IMMC) & Earth
18 and Life Institute (ELI), 4 avenue Georges Lemaître, B-1348 Louvain-la-Neuve, Belgium

19 ⁸ Delft University of Technology, Delft Institute of Applied Mathematics (DIAM), Van Mourik Broekmanweg
20 6, 2628XE Delft, The Netherlands

21

22 * Correspondence: nicolas.gratiot@ird.fr; Tel.: +84-9-4129-4232

23

24 **Abstract:** The Mekong river is one of the largest rivers in the world, which flows through
25 six countries of Southeast Asia (China, Myanmar, Laos, Thailand, Cambodia and Vietnam).
26 Its hydro-sedimentary regime is changing rapidly, as a consequence of a regional shift of
27 land use (agriculture, road, etc.), damming, sand mining and climate changes, among others.
28 This study assesses the behavior of particles transported in suspension in the Lower Mekong
29 River (LMR), along approximately 1700 km from fluvial to estuarine environments.
30 Suspended sediment properties were estimated, simultaneously with hydrodynamic
31 conditions, during three field campaigns. In addition, further investigations were performed
32 in the laboratory to assess the structures of particles (flocculated or not), their capacity to
33 flocculate (and the impacts on siltation), under a wide range of sediment concentration (400
34 to 4000 mg.L⁻¹). This study confirms that suspended sediment transported in the LMR are
35 predominantly (75 % by volume) flocculi (or freshly eroded soils aggregates), with median

36 aggregated particle size in the range 10 - 20 μm and median settling velocity of the order of
37 $0.01 - 0.1 \text{ mm.s}^{-1}$. These flocculi are robust under the hydrodynamic conditions (turbulence
38 and suspended sediment concentration – SSC) existing in the LMR. Laboratory
39 investigations reveal the existence of a threshold sediment concentration (400 mg.L^{-1}),
40 beyond which flocculation and sedimentation increase of orders of magnitudes. Thus,
41 concentration that exceeds this threshold might promote the formation of so-called fluid mud
42 layers. Because of the nonlinear response of flocculation and sedimentation with SSC and
43 considering the ongoing changes at a regional scale in the LMR, higher occurrence of fluid
44 mud layers in the fluvial upstream waterbodies might be anticipated, and a lower occurrence
45 in estuaries and alongshore where the concentration decrease. The geomorphology could be
46 impacted, with an over-siltation in dams and an exacerbated erosion of the muddy-mangrove
47 coast.

48 **Keywords:** Mekong; LISST; SCAF; fluid mud layer; flocculation, settling velocity

49

50 **1. Introduction**

51 The Mekong river is the tenth longest river in the world with a length of 4909 km and has a
52 basin area of $795,000 \text{ km}^2$. Its mean annual discharge is approximately 475 km^3 , i.e. the sixth
53 largest in the world. The river originates from the Tibetan Plateau (China) with an elevation of
54 more than 5000 m above sea level (a.s.l.); then, the river flows through a variety of
55 geomorphological and climatic systems and ends in the fertile delta of Vietnam ($55,000 \text{ km}^2$),
56 before discharging into the South East Sea of Vietnam (Mekong River Commission portal -
57 MRC, www.mrcmekong.org/). Under human pressures and climate change, the river is facing
58 many serious issues in link with changes in sediment dynamics. One of the most evident
59 transformation is the construction of large hydropower dams in the upstream Mekong, which
60 are modifying the hydrological cycle, and reducing the sediment discharge into the floodplain
61 and estuaries at an alarming point (Schmitt et al., 2017). Sand mining in the delta is also a
62 direct threat for the hydro-sedimentary budget. According to the literature, sediment flux has
63 already decreased by almost five fold over 35 years, from about $160 \text{ mill. tons.year}^{-1}$ in 1983
64 (Milliman et al., 1983) to $87.4 \pm 28.7 \text{ mill. tons.year}^{-1}$ in 2005 (Darby et al., 2016 and Schmitt
65 et al., 2017) and $40 \pm 20 \text{ mill. tons.year}^{-1}$ in 2015 - 2016 (Thi Ha et al., 2018).

66 Sand mining, trapping by dams, and the resulting reduction of sediment flux are undoubtedly
67 corroborated with some changes in the nature (and populations) of particles transported. Some
68 expected consequences in geomorphology, floodplain fertility and pollutant dynamics are
69 already evoked (Kondolf et al., 2018), but need to be better studied. Previous studies
70 conducted in the LMR indicated that the upper fluvial section was dominated by two particles
71 size populations: silts, with a diameter of 10 - 20 μm ; and sands, with a diameter of 63 - 200
72 μm , accounting for 78 % and 22 % of the total particle load, respectively (Peteuil et al., 2014).
73 Downstream, in the estuary, flocculated fine particles dominate. The observed floc size,
74 reported in the literature, was 30 - 40 μm , constituting 60 - 80 % of the total sediment load in
75 high flow season. However, in the low flow season, the floc size increased to 50 - 200 μm ,
76 accounting for 70 - 80 % of the total volume (Wolanski et al., 1996 and Wolanski et al.,
77 1998). This observed variability of sediment properties reflects a direct adjustment of physical
78 properties along streams, which operates at microscopic scales (flocculation, sedimentation
79 and erosion), in link with hydrodynamic conditions and their seasonal variations. The
80 different origins, together with different physicochemical and biological conditions between
81 the sites, cause difficulties in interpreting the results.

82 Particle size, settling velocity and their spatio-temporal evolution through flocculation, are
83 fundamental properties that need to be estimated to assess sediment transport and deposition
84 processes in space and time (Manning et al., 2011a; Winterwerp, 2002). This is particularly
85 true in the case of mud/sand mixtures, where complex interactions occur and need to be
86 characterized for a realistic understanding of sediment dynamics (Manning et al., 2010).
87 Conceptually, flocculation develops from primary particles into hierarchical structures,
88 namely flocculi, microflocs and macroflocs. Primary particles mainly consist of fine particles
89 with sizes of 1 - 6 μm , and can be organic or inorganic. They aggregate to form 1st order
90 structures, so-called flocculi, with diameters of the order of 6 - 50 μm . They are usually
91 hardly broken down into primary particles, even at the highest turbulent shear modulus
92 experienced by particles in large rivers. Thus, it is generally considered that flocculi are a
93 major component of sediment dynamics. Microflocs form the 2nd order of aggregation. They
94 include primary particles and flocculi and have sizes of 50 - 200 μm . Finally, macroflocs are
95 the largest particle structures. They are loose structures with a wide size distribution, ranging
96 from hundreds to thousands of micrometers (Lee et al., 2012 and Fettweis et al., 2006). Flocs
97 (micro and macro) are generally fragile structures, easily broken down when passing through
98 high turbulent shear modulus (Manning et al., 2011a).

99 Flocculation at microscopic scale, as some hydro-sedimentary and geomorphological impacts
100 at scales of river reaches, estuaries and deltas, in particular because it promotes the formation
101 of fluid mud layers. Fluid mud is defined as a mixture of high-concentrated fine sediments
102 with water (Bachmann et al., 2005). It is generated by liquefaction of cohesive sediment beds
103 by waves or by an imbalance between settling and eddy diffusion near the bed, or by the
104 convergence of sediment fluxes from upstream and downstream. In energetic environments,
105 large particles such as sand are also found in fluid mud samples, but the portion is less than
106 few percent (McAnally et al., 2007). Fluid mud masses may be advected over large distances
107 horizontally without losing their coherent nature or internal chemical properties; and its
108 horizontal convergence may often be a key mechanism of their accumulation (McAnally et
109 al., 2007). Thus, fluid mud in thin layers is considered as an intermediate stage of deposition
110 (before formation of consolidated bed layers) or bed erosion (under entrainment process by
111 fluidization (McAnally et al., 2007). Its thickness varies from few centimeters to meters
112 (Sottolichio et al., 2011; Azhikodan et al., 2018).

113 The occurrence of fluid mud is commonly observed in quiescent environments such as lakes
114 and reservoirs (Mehta et al., 1991; McAnally et al., 2007) or in the Estuarine Turbidity
115 Maximum zones (ETM) (Uncle et al., 2006; Winterwerp et al., 2011; Azhikodan et al., 2018)
116 such as estuaries, navigation channels, harbour basins or along muddy coasts all over the
117 world (Bachmann et al., 2005; Schelske et al., 2006; Gratiot et al. 2007; Toorman et al. 2018).
118 The turbidity maximum zone is often created by resuspension from the bed during parts of the
119 tidal cycle and shows a significant drag reduction at high SSC concentration gradient (Dyer et
120 al., 2002a and Dyer et al., 2002b). However it has been poorly studied and reported in the
121 literature dedicated to the LMR (Wolanski et al., 1998, Xue et al., 2010) and received some
122 more interest recently (Gugliotta et al., 2019; Nittrouer et al., 2017; Gratiot et al., 2017).

123 This study originally combines in situ measurements and laboratory investigations to examine
124 the physics of particles (especially flocculation properties, measured with new patented
125 equipment developed by SCAF[®]) and to understand transport/deposition processes in the
126 LMR. Sampling and analyses are performed in three contrasted environments: an upper
127 fluvial reach in Laos (Fig. 1b), a lacustrine environment in Cambodia (Fig. 1c) and an
128 estuarine environment in Vietnam (Fig. 1d). The same methodology was applied for these
129 three contrasted environments (upstream river, lake and estuary). Results obtained allow for
130 answering and discussing the following points:

- 131 • Are suspended sediment flocculated or not (percentages of cohesive versus non-
132 cohesive particles transported in suspension)?
- 133 • If yes, are floc populations stable from upstream to downstream and/or highly
134 dependent on hydrodynamic conditions (SSC, turbulence, salinity)?
- 135 • Are suspended sediment predominantly transported as washload (single path with no
136 bed interactions), or does it experience successive phases of deposition and erosion?
- 137 • How much SSC increase can modify flocculation, sedimentation and how much this
138 could contribute to the formation of fluid mud layers and, finally, modify the
139 geomorphology of the LMR?

140 By answering to the four questions above, the paper proposes a better understanding of the
141 physical properties of sediment and their transportation modes along the Lower Mekong
142 River. Because flocculation and fluid mud layers are playing an important role in the dynamic
143 of the Mekong Delta, this information will facilitate the implementation of integrated tools,
144 such as ecological/geomorphological models, to go through a better management of large
145 scale hydrosystems.

146 **2. Study areas and Methods**

147 *2.1. Study area*

148 Field investigations have been conducted at three locations of the LMR, assumed to be
149 representative of river morphological units, from the upper fluvial environment to the
150 lacustrine and the estuarine environments (Fig. 1a).

151 2.1.1. Fluvial environment

152 The upper fluvial reach considered is located at the level of Luang Prabang city, Laos
153 (Fig.1b). It is situated on a long stem at the confluence of the Mekong and Nam Khan rivers, a
154 tributary of the Mekong. Its altitude is approximately 300 m a.s.l. This area is covered with
155 steep hillsides and has been experiencing drastic land use changes, predominantly leading to
156 erosion, since the last decades (Ribolzi et al., 2017). At Luang Prabang, the Mekong river
157 section is already wide, with width of 600 - 700 m. However, when passing through gorges,
158 the channel becomes swiftly narrow, approximately 100 m wide, and bounded by limestone

159 pavement. The channel has a median depth of around 10 m, with maximum depth of
160 approximately 30 m (Gupta et al., 2007).

161 The field survey was conducted for 8 days, from 26 June to 2 July 2017, at the beginning of
162 the wet season. There were neither extreme floods nor low water situations, thus the
163 hydrodynamic conditions were suitable for sampling and analysing a typical (median)
164 suspended sediment distribution in the river. Twenty-seven samples were taken in the main
165 Mekong river and its tributaries (Nam Ou, Nam Suang and Nam Khan tributaries). During the
166 survey, hydro-sedimentary conditions were also characterized on two cross-sections with
167 distances of approximately 20 km (Fig. 1a, see section 2.2.3). For each location, samples were
168 collected in three vertical profiles (left bank – V1, middle bank – V2 and right bank – V3). In
169 each vertical profile, 3 litres of water sample were taken at various depths (0.1 h, 0.4 h, 0.7 h
170 and 0.9 h, h being total water depth).

171 2.1.2. Lacustrine environment

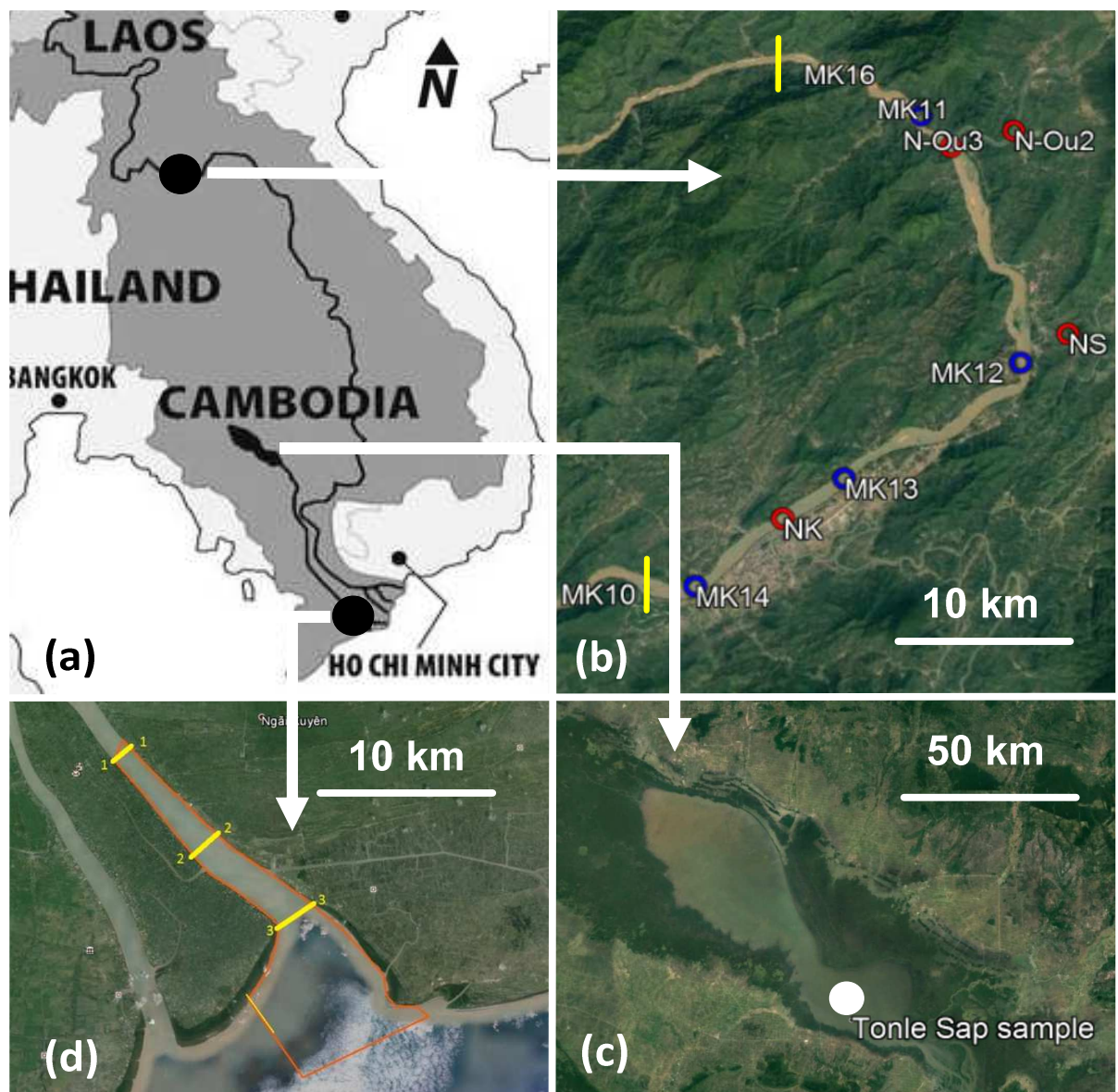
172 With volume of 1.8 – 58.3 billion m³, the Tonle Sap lake is the largest freshwater source in
173 Southeast Asia (Kummu et al., 2014). It is located in the Cambodian floodplain (Fig. 1c) and
174 comprises a permanent waterbody, twelve tributaries, extensive floodplains and the Tonle Sap
175 river linking the lake to the Mekong river (Kummu et al., 2014). At the confluence, the river
176 splits into the Bassac river (Hau river) in the West and the Mekong river (Tien river) in the
177 East. The Tonle Sap system has strong and original hydrodynamic relationships with the
178 Mekong mainstream (Kummu et al., 2008). During the wet season, flooding from the Mekong
179 river causes a reverse flow direction, into the Tonle Sap lake. The lake area then increases
180 from 2500 km² to approximately 15000 km², while the depth rises from 1 to 9 m. At the
181 opposite, the slow release of floodwaters from the lake during the dry season is a very
182 important water source to sustain the river discharge of the Mekong delta (Hai et al., 2008). In
183 this specific paper, we focus on the physics of particles. The field survey was performed for 9
184 days from 13 October to 21 October 2018, during high flow season. The material used is
185 freshly deposited sediment, collected near the Mekong river tributaries, after a flood season at
186 the bottom layer.

187 2.1.3. Estuarine environment

188 The Mekong delta (MD) is situated at the most Southeast part of the LMR (Fig. 1d). It covers
189 approximately 55,000 km² (Balica et al., 2014), extending from the Cambodia - Vietnam
190 border to the Gulf of Thailand and the East Sea of Vietnam (Tran et al., 2018). Together with

191 the Mekong river and the Bassac river, it separates into eight tributaries (Hung et al., 2014)
192 before discharging into the East Sea (Wolanski et al., 1996 and Xing et al., 2017). At the
193 interface between land and the sea, the estuary is strongly impacted by both flooding from
194 upstream and the tidal flows, as well as wave forcing (Gugliotta et al., 2019).

195 Three surveys with contrasted seasonal conditions were conducted in the Song Hau estuary
196 (as part of the Lower Mekong Delta Coastal Zone project), in December 2015, March and
197 October 2016. During these surveys, three cross-sections (upstream - T1, middle - T2,
198 downstream - T3), with distances of 10 and 15 km, respectively, were chosen to monitor and
199 assess the impact of saline water intrusion on flocculation (Fig. 1d and sketch of Fig.6). At
200 each location, samples were taken in three vertical profiles. In total, 104 samples with volume
201 of 5 litres per sample were collected to investigate the spatio-temporal dynamics of suspended
202 sediment for contrasted sediment concentration (SSC) and turbulent levels.



203

204 **Fig. 1.** Domains of interest [a] (Smardon et al., 2009). Sampling sites and locations in fluvial
 205 (Luang Prabang, Laos with blue dots reporting samples in main stream, red dots reporting
 206 samples in tributaries and yellow segments reporting cross-sections [b]), lacustrine
 207 environment (Tonle Sap floodplain, Cambodia with white dots showing the sampling location
 208 [c]), and estuarine environment (Song Hau estuary, Vietnam with yellow segments reporting
 209 cross-sections and red lines showing the local domain [d]).

210 *2.2. Methods*

211 The suspension regime of the sediments transported in a flow strongly depends on interactions
 212 between hydrodynamics, particle size, density and settling velocity. Thus, the understanding
 213 of particle size distribution (PSD) of suspended particulate matter (SPM) is one of
 214 prerequisites to properly simulate sediment dynamics (Fennessy et al., 1994). This study

215 originally proposes a direct estimation of settling velocity and flocculation with the patented
216 SCAF instrument (System for the Characterization of Aggregates and Floccs, Gratiot et al.
217 2015).

218 The five sections hereinafter describe the methodology adopted to measure the physical
219 properties of suspended sediment and evaluate its transport dynamics. The instruments at our
220 disposal are particularly relevant to estimate both particle size and settling velocity, but it was
221 not possible to measure directly the density of floccs, which may be seen as a limitation.

222 2.2.1. A portable mixing tank device to reproduce natural inflow turbulent conditions

223 To measure PSD under turbulent conditions close to the ones experienced by natural rivers, 2
224 litres of water samples were introduced into a portable rectangular-base mixing jar tank (with
225 diameter of 11.5 x 11.5 x 15 cm), and then mixed with an impeller for thirty minutes. Since
226 the work of Gratiot and Manning (2004), this mixing duration is assumed to ensure a good
227 homogenization of the fluid mud mixture, and a dynamic equilibrium between the rate of
228 flocculation and breakage. Some details on the experimental set-up can be found in Gratiot et
229 al. (2017). During preliminary experiments, an Acoustic Doppler Velocity Profiler (Nortek
230 Vectrino2) was immersed in the mixing tank filled with clear water, in order to measure
231 the 3D turbulent field of velocity and deduce the mean turbulent energy dissipation rate G (s^{-1})
232 ¹). With a rotation speed of 100 rpm, G was about $44 s^{-1}$, which corresponds to high shear rate
233 conditions, such as observed near bottom in natural rivers and estuaries (Gratiot et al., 2017).
234 For further details on the mixing tank device, the reader can refer to Gratiot et al. (2017,
235 supplementary information).

236 2.2.2. PSD measurements and characterization of the particle-classes/population/group?

237 To characterize the different populations of particles, the terminology of Lee et al. (2012) is
238 used. It is based on four classes, namely primary particles, flocculi, microflocs and macroflocs
239 (as mentioned in the Introduction section). We utilize the LISST-Portable XR instrument to
240 measure sediment particle sizes during mixing. The operational principle of the LISST-
241 Portable XR is based on laser light scattering (or laser diffraction). This instrument provides
242 the logarithmical PSDs over 44-size bands in the ranges of particle size from 0.35 to 500 μm
243 by using the Fraunhofer approximation or the exact Lorenz-Mie theory. The volumic
244 concentration is in micro-litre/litre ($\mu L.L^{-1}$), corresponding to sediment concentration of 30 -
245 1900 $mg.L^{-1}$ in the chamber of measurement. Each spectrum shows independent semi-log
246 distributions of sub-populations, that were characterized by their mean particle size D_f , their

247 standard deviation σ_{Df} and their relative volumetric concentration. The operating range of
248 optical transmission recommended by LISST-Portable XR is 75 - 95 %. For optical
249 transmission lower than 75 %, multiple-scattering can bias the signal and lead to an
250 underestimation of the size distribution.

251 This device has been utilized successfully in many contrasted environments, such as the
252 Saigon - Dong Nai rivers, Vietnam (Nguyen et al., 2019), a hydropower plant in Malaysia
253 (Azrulhisham et al., 2018), Northern French Alps (Antoine et al., 2015) and Philadelphia
254 (Windt et al., 2017), among others.

255 It is worth noting that many other techniques exist to measure PSD, particularly video-based
256 techniques, such as the immersed INSSEV instrument (Fennessy et al., 1994) or the LabFlocs
257 portable video system (Manning et al., 2007). All methods have advantages and
258 disadvantages, so that a combination of different techniques is probably the best efficient.

259

260 For describing PSDs of primary particles, flocculi, microflocs and macroflocs, we apply a
261 mathematical function to separate the signal into four log-normal distribution (Mikkelsen et
262 al., 2006). Such post processing is also useful to prevent misinterpretation, resulting from air
263 bubbles and other artefacts that can be observed in the raw particle size spectrum (Sequioa,
264 2016).

265 In this study, the PSD of each sample was measured in two steps, before and after two
266 minutes of sonication, for a mechanical particle breakage under acoustic waves. Hence, it is
267 possible to assess the proportion of sand and flocs because large-size particles built by smaller
268 cohesive particles (silt or clay) are, at least partially, dispersed by sonication (Gratiot et al.,
269 2017) while the sand particles are indivisible and then maintain a constant diameter after
270 sonication.

271 2.2.3. Characterization of the settling and flocculation regimes

272 Depending on SSC, three settling regimes can be observed for natural sediment in aquatic
273 environment (Van Leussen, 1994), namely (1) free settling, (2) flocculation and (3) hindered
274 regimes. For the lowest SSC, flocculation is weak and particles are settling almost
275 independently from each other (free settling regime). Particle settling velocity can then be
276 broadly estimated by the Stokes' law or derived laws as the sum of individual particles
277 settling down (Stokes, 1857; Winterwerp, 2002). The flocculation settling regime occurs with
278 midrange of SSC (tens to hundreds of mg.L^{-1}). The settling velocity of cohesive and mixed
279 fine-grained sediments then becomes more complex because it is influenced by both particle

280 interactions and individual properties (Manning et al., 2010), as well as turbulent shear
281 (Winterwerp, 2002; Manning et al., 2011a). Flocculation is promoted, which results in larger
282 particle sizes and higher settling velocities (Droppo et al., 2005). The hindered settling regime
283 occurs at very high SSC (several grams per litre or more), and settling mostly occurs by mass,
284 depending on the cohesion and suspension concentration (Camenen and Van Bang, 2011; Van
285 and Van Bang, 2013).

286 To assess the settling velocity w_s ($\text{m}\cdot\text{s}^{-1}$) (and flocculation) for all these regimes in natural
287 environment, we used the System for the Characterization of Aggregates and Flocs (SCAF), a
288 recently patented instrument (Gratiot et al., 2015) that was successfully applied in some recent
289 researches (Wendling et al., 2015, Gratiot et al., 2017, Legout et al., 2018, Nguyen et al.,
290 2019). This instrument is a glass settling column with dimension of 20 cm high and 3.5 cm in
291 diameter, equipped with 16 infrared ($\lambda = 980$ nm) emitters and 16 diametrically opposed
292 photo-sensors measuring at a frequency of 210 Hz. SCAF instrument measures the light
293 attenuation in the settling tube with depth and time during the deposition of particles (Gratiot
294 et al., 2015). Sensors are located every 1 cm down the column with the lower sensor located at
295 1 cm above the bottom of the column. Measurements taken in the eight upper centimeters of
296 the SCAF settling tube provided an estimate of flocs settling velocity under quiescent
297 conditions, denoted $w_{s,q}$ ($\text{m}\cdot\text{s}^{-1}$) while measurements realized in the eight centimetres near the
298 bottom of the settling tube provided an estimation of flocs settling velocity after flocculation
299 by differential settling under settling dominated conditions, this latter velocity being reported
300 as $w_{s,\neq}$ (Wendling et al., 2015). In the case of non-cohesive particles, such as sand or silt, or
301 clay particles with deflocculant, the settling velocity does not change during settling; $w_{s,q}$ and
302 $w_{s,\neq}$ are similar and the flocculation index $\text{FI} = (w_{s,\neq} - w_{s,q}) / w_{s,q}$ is close to zero (Wendling et
303 al., 2015). As SCAF instrument is based on by mass sedimentation of a fluid mud mixture in a
304 settling tube, it is inherently affected by the shape, density and compositions of all particles
305 presented in the sample.

306 2.2.4. Other hydrodynamic measurements

307 Complementary measurements were performed during field surveys. An Acoustic Doppler
308 Current Profiler (ADCP), an Hydrolab probe (a multi-parameter probe measuring in-situ
309 water quality parameters), SSC samplers and a EUTECH turbidimeter were used to
310 characterize the water flow in the cross-sections, suspended solid concentration and physical
311 parameters such as turbidity, temperature, pH, ORD, EC, salinity, etc. An YSI multi-

312 parameter probe (Water Quality Sampling and Monitoring Meters and Instruments) was also
313 used to check the average values of the measured physical parameters.

314 2.2.5 Characterization of the suspension regime

315 In order to characterize the suspension regime, the non-dimensional Rouse number (Rouse,
316 1937), which express the balance between the upward turbulence forces (u_*) lifting the
317 particles and the gravity forces applied (W_s) on the same particles in a river stream, was
318 calculated for each flow condition encountered. The Rouse number is calculated as following:

$$319 \quad R_o = \frac{w_s}{\beta \kappa u_*} \quad (1)$$

320 where the settling velocity w_s is inferred from the SCAF results (Fig. 5), or calculated by the
321 Stokes' Law from the PSD measurements. κ is the von Kármán constant, taken equal to 0.41.

322 The constant of proportionality β is the ratio of sediment to eddy diffusivity, describing the
323 diffusion patterns of a fluid particle and a sediment particle. In water environment, it is often
324 assumed that eddy viscosity is equal to eddy diffusivity, thus value β is typically
325 hypothesised to be one (Rijn, 1984; Farrell and Sherman, 2013). u_* ($\text{m}\cdot\text{s}^{-1}$) is shear velocity.
326 In the fluvial and estuarine environments, the shear velocity u_* was computed by using the
327 ADCP, with the assumption that the velocity profiles follow the logarithmic inner-law (so-
328 called "Law of the Wall") (Sime et al., 2007; Santini et al., 2019, Eidam et al., 2017). In the
329 lacustrine environment, u_* was computed from 2D hydrodynamic simulation results by the
330 Second-generation Louvain-la-Neuve Ice-ocean Model (SLIM, <https://www.slim-ocean.be/>).

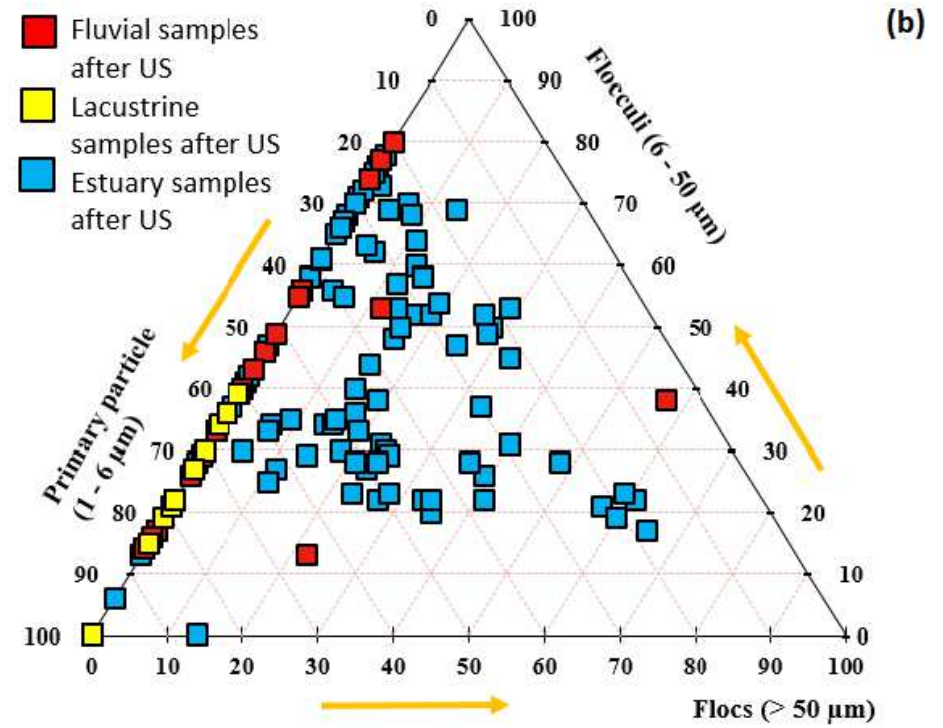
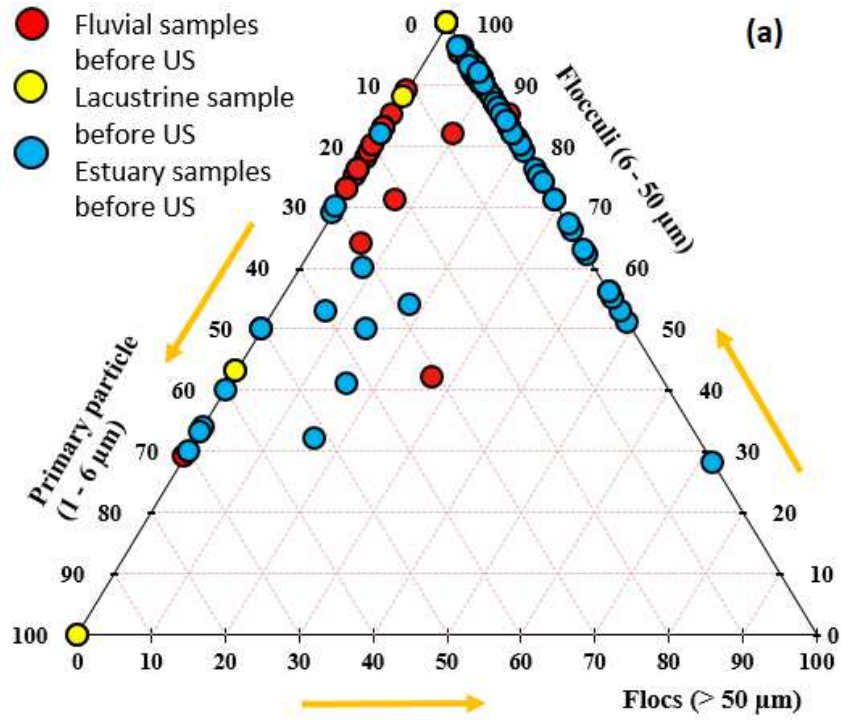
331 The application of Eq.1 to characterize the suspension regime is relevant, but we should
332 underline that uncertainties can be high, as both W_s and u_* are hardly estimate in the field.

333 3. Results

334 3.1. Particle size distribution (PSD)

335 The PSD of all samples are gathered in a triangle sketch in Fig. 2. Before sonication, most of
336 the particles are flocculi with an average contribution percentage of 46 %, 78 % and 78 %, for
337 fluvial, lacustrine and estuarine environments, respectively (Fig. 2a). After sonication, the
338 PSD displayed an increased number of primary particle class for all samples (51 %, 67 % and

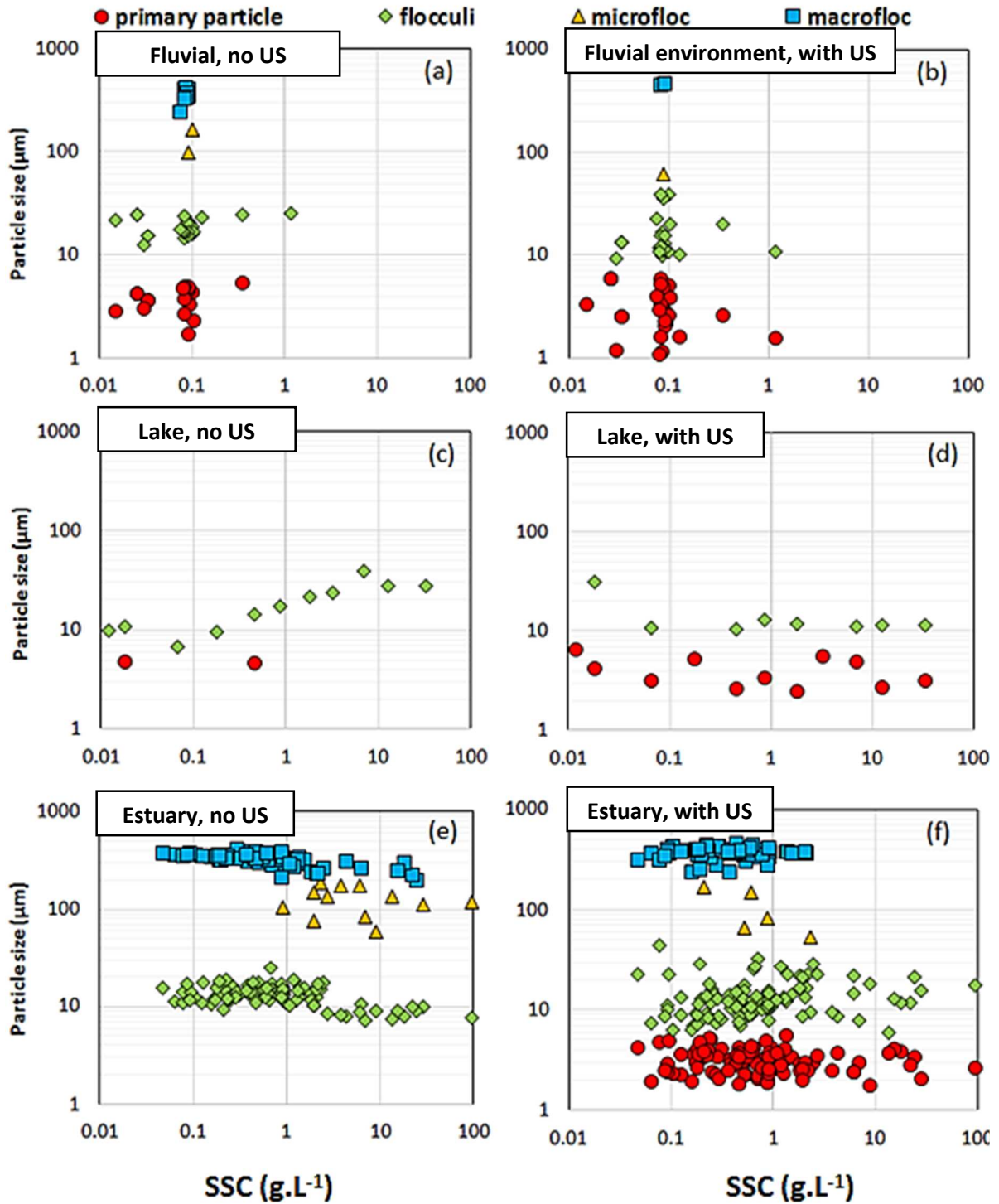
339 32 %, respectively), while it witnessed the reduction in the percentage of flocculi and flocs
340 (Fig. 2b). This figure also shows a wider diversity of particle sizes in the Mekong estuary
341 (blue circles and squares) than in the lacustrine and the fluvial environments (yellow and red
342 circles, respectively). It illustrates that estuaries are complex and changing environments,
343 which mix both fluvial and coastal water (see the sketch in Fig.6 and the corresponding
344 discussion section). In the case of the Mekong estuaries zone, sediment transport and
345 deposition is strongly affected by fluvial inflow, tidal currents, but also resuspension of
346 particles by wind-induced current, waves and coastal oceanic currents (Gugliotta et al., 2019;
347 Marchesiello et al., 2019).



348

349 **Fig. 2.** Triangulars of PSD in upper parts and estuary analyzed (a) before and (b) after sonication

351 Fig. 3 aims at highlighting the role played by SSC on flocculation of particles. This figure
 352 gathers both data collected in the field and in the laboratory, before and after sonication.



353

354 **Fig. 3.** Variation of particle classes with SSC in fluvial environment, lacustrine environment

355 and estuary before and after sonication

356 3.2.1. Particle size populations in the fluvial environment (Laos)

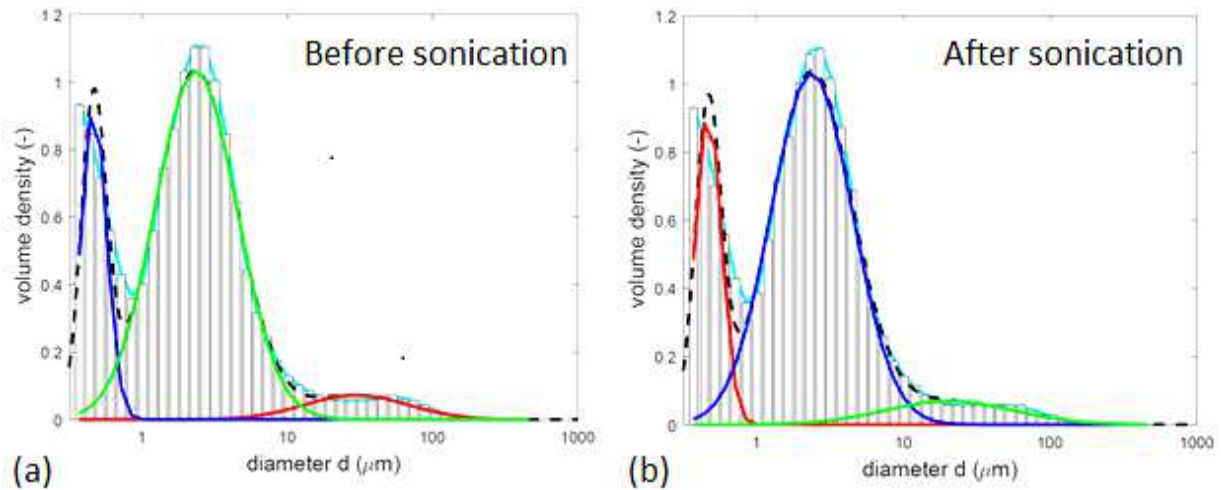
357 Fig. 3 (a) and Fig. 3 (b) present the PSD of particles populations sampled in the fluvial
358 section. On average, the primary particles accounted for 37 % of all particle population (in
359 volumetric concentration). The predominant population is flocculi, with a volume
360 concentration of approximately 46 %. Microflocs and macroflocs were fewer and accounted
361 for (only) 3 % and 14 % of the total volume, respectively. The macroflocs size reached a
362 median diameter of 422 μm . Fig. 3 (b) shows the PSD plot after sonication. The sonication
363 broke up particles so that the percentage of primary particles increased (+14 %) to 51 % and
364 flocculi decreased slightly (-5 %) to 41 %. The percentage of microflocs remains stable and
365 small (approximately 2 %), and the percentage of macroflocs decreases by more than two
366 folds (to approximately 6 %). These coarsest particles were not all broken up by sonication,
367 which indicates the presence of sand. The samples issued from the tributaries had generally
368 similar PSDs than the ones in the mainstream. After sonication, PSD of these samples still
369 exhibits high values, with a maximum diameter of 347 μm . It means that these water samples
370 contains predominantly sand, which is in agreement with visual observations during field
371 campaigns. A detailed examination of PSD before and after sonication confirmed that samples
372 in fluvial environment consisted of both cohesive sediment and sand particles. These PSDs
373 are in agreement with the results of Camenen et al. (2014).

374 3.2.2. Particle size populations in the lacustrine environment (Tonle Sap, Cambodia)

375 In the lacustrine environment, only two particles classes (primary particles and flocculi,
376 without flocs and no sands) appear. Before sonication (see Fig. 3c), the percentage of primary
377 particles and flocculi accounts for 22 % and 78 %, respectively. After sonication (see Fig. 3d),
378 these percentages reverse with a predominance of primary particle (67 %) and a simultaneous
379 decrease of flocculi (33 %). The particle size in the lacustrine environment were smaller ($7 \pm$
380 $3 \mu\text{m}$) than in the fluvial part ($18 \pm 5 \mu\text{m}$). Fig. 3c exhibits a clear rise (3 to 4 folds) of flocculi
381 size with higher SSC, as a response of flocculation of primary particles (or colloids) on
382 flocculi.

383 Interestingly, colloids were observed in some samples taken in the Tonle Sap, with diameters
384 of $< 1 \mu\text{m}$ (see Fig 4). After 12 hours of deposition in the mixing tank at rest, the particles still
385 in suspension were both colloids with diameter of approximately 0.45 μm , which are
386 consistence with a research conducted by Seah et al 2017, accounting for 21 %; primary

387 particle (73 %) and few flocculi (6 %). After sonication, the structure of sediments presents
 388 the same pattern (21 % of colloid, 72 % of primary particles and 7 % of flocculi). This can be
 389 explained by a stable mixture of this sediment classes, which are hardly broken down into
 390 smaller particles even after sonication. Colloids play an important role and act as “catalyzers”
 391 of the interaction between sediment and substances in the water such as substance dissolved
 392 matter, substance from precipitation, absorbed ions and organic matters (Wendling et al.,
 393 2015).



394 **Fig 4.** PSD of a sample in the Tonle Sap before (a) and after sonication (b). The first peaks in
 395 two graphs show the appearance of colloids with diameter of $< 1 \mu\text{m}$.
 396

397 3.2.3. Particle size populations in the estuarine environment (Song Hau river, Vietnam)

398 Fig 3 (e and f) display the PSD in the estuary versus SSC before and after sonication,
 399 respectively. Once again, flocculi is the dominant population of particles, with mean diameter
 400 of approximately $15 \mu\text{m}$ (in range of $8 - 20 \mu\text{m}$), accounting for 80 % of total volume. Before
 401 sonication, only three classes of particle sizes exist in the estuarine samples, flocculi,
 402 microflocs and macroflocs. The prevailing fine silt population shows mean diameter of $7 -$
 403 $12.5 \pm 10 \%$ μm , that constituted 83 – 94 % of total volume. Diameters of coarser population
 404 were in the range of $112 - 310 \pm 10 \%$ μm . After sonication, particle size reduced
 405 significantly. A group of primary particles (red circles), which were completely absent from
 406 the PSDs before sonication, appears in almost all samples, which undoubtedly demonstrates
 407 the cohesive nature of sediments in the estuary. Due to breakage into smaller particles under
 408 turbulence shear, diameters of fine particles (primary particles and flocculi) reduce to $1.8 - 4$
 409 $\pm 10 \%$ μm and $6.3 - 12.2 \pm 10 \%$ μm , respectively while the size of coarse particle

410 (microflocs) falls to $15 - 65 \pm 10 \%$ μm . A population of sand particles (with diameter > 200
411 μm), not broken-up with/after sonication, is also evidenced.

412 *3.3. Settling velocity*

413 Fig. 5(a) shows the variation of suspended sediment settling velocity with SSC, measured
414 directly with SCAF instrument. For the three aquatic environments, settling velocity rises with
415 SSC because of flocculation process. Even if there are only 5 SCAF samples in the fluvial
416 environment, 9 samples in lacustrine environment, 19 samples in the estuary, the three curves
417 exhibit similar trends, which support the existence of free settling, flocculation and hindered
418 regimes, as previously depicted by Wendling et al. (2015).

419 The free settling regime is observed for the lowest SSC (tens of mg.L^{-1}). Sediment settling
420 velocity measured in the fluvial, lacustrine and estuarine environments are of the same order
421 of magnitude, the mean settling velocities being approximately $0.02 - 0.08 \text{ mm.s}^{-1}$ in the
422 fluvial section, $0.05 - 0.06 \text{ mm.s}^{-1}$ in the lake, and $0.01 - 0.02 \text{ mm.s}^{-1}$ in the estuary. The
423 widest range of settling velocities observed in the fluvial environment is probably the
424 fingerprinting of a wide variety of compact soil aggregates, freshly eroded from the
425 watershed, and not yet at equilibrium with the prevailing hydrodynamic conditions, as
426 reported conceptually by Droppo et al. (2015). In this free settling regime, particles settle
427 almost independently, the interaction between particles is poor, which is reflected by a
428 moderate flocculation index (FI lower than 2) in all SCAF measurements (in Fig. 5, right
429 panel). Flocculation predominates in the range of $0.4 - 4 \text{ g.L}^{-1}$, thus the settling velocities of
430 fluvial, lacustrine and estuarine sediments rise up to 0.2 mm s^{-1} , $0.1 - 2 \text{ mm.s}^{-1}$ and $0.03 - 0.8$
431 mm.s^{-1} , respectively.

432 In the lacustrine environment, a significant rise of settling velocity is found with higher SSC.
433 The SCAF results show that the settling velocity of the lacustrine environment reaches the
434 peak of 2.0 mm.s^{-1} when SSC reach approximately 2.0 g.L^{-1} .

435 In the estuary, the complex hydraulic regimes, including resuspension of freshly deposited
436 sediments (Marchesiello et al., 2019) and the mixing between fresh water and saline water led
437 to the formation of a zone of turbidity maximum and promote the formation of flocs (both
438 microflocs and macroflocs) (Dyer et al., 2002a and Manning et al., 2007). As a consequence,
439 the settling velocity also increases (Dyer et al., 2002b and Manning et al., 2011b). Beyond 4.0
440 g.L^{-1} , hindered regime becomes predominant. It implies the decline of settling velocity in the

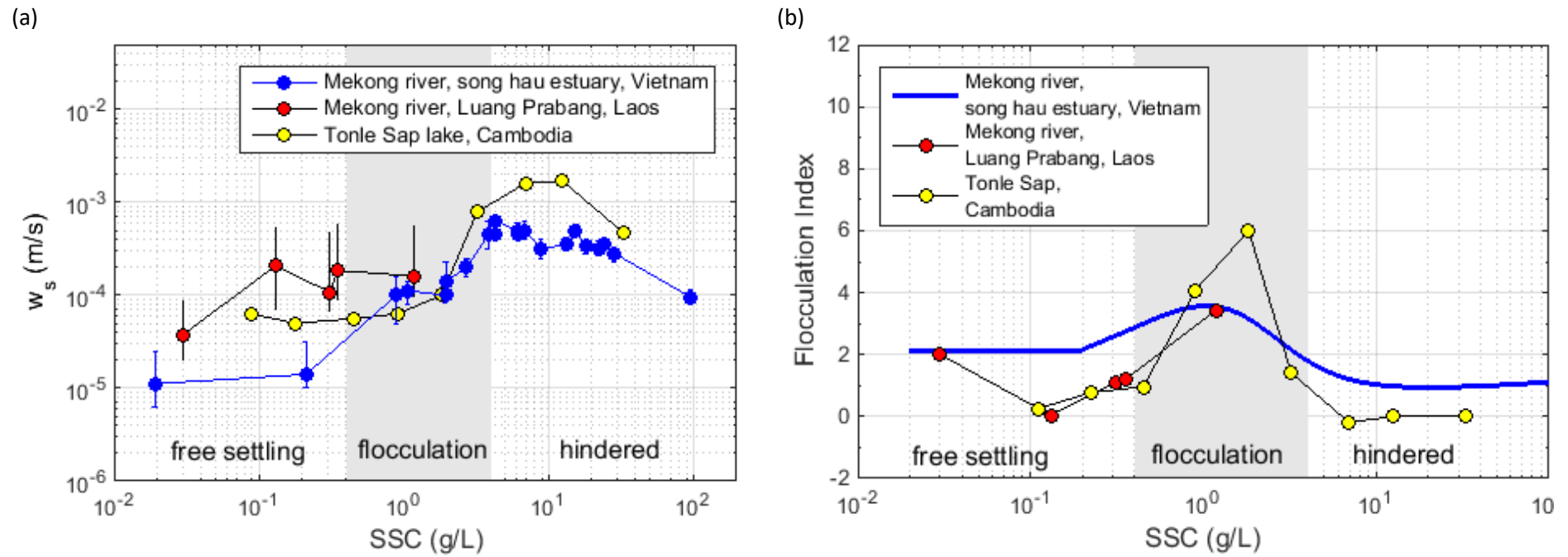
441 lacustrine and estuarine environments, from 2.0 to 0.4 mm.s⁻¹ and from 0.8 to 0.1 mm.s⁻¹,
442 respectively.

443 The main difference of these three environments is that flocculation processes seem to appear
444 at lower concentration in the fluvial environment (approximately 20 - 30 mg.L⁻¹) than in the
445 lake (approximately 1 - 2 g.L⁻¹) or in the estuary (approximately 300 mg.L⁻¹). We cannot
446 exclude that the particles sampled in the fluvial environment are not real flocs, but correspond
447 to soil aggregates that are not in equilibrium with their hydraulic environment (Droppo et al.,
448 2005).

449 The flocculation efficiency is higher for the estuarine environment (+ 60 % of increase of the
450 settling velocity) and highest for lacustrine environment (+200 % of increase) than for the
451 fluvial environment (+7 % of increase).

452 Concerning the Flocculation Index (FI), sediment samples in the river and in the lake (red
453 circles for fluvial environment and yellow circles in lacustrine environment, see Fig. 5b)
454 exhibit a high dynamic, even in fresh water. The highest rate of flocculation is observed in the
455 lacustrine environment, where the measured FI increases from 0 to 6, when SSC increases
456 from 0.1 to 3.0 g.L⁻¹. Interestingly, after getting the FI peak of 4 – 6, the efficiency of
457 flocculation in the lacustrine environment fell to value of 0 – 1.75. It means that flocculation
458 still occurs, but the volumetric concentration of particles is so high that the settling velocity
459 cannot increase anymore. Settling velocity of small particles is hindered by the high SSC,
460 whereas colloids are trapped on the surface of larger particles (Comba et al., 2009).

461 The estuarine sediments also experience three settling regimes with FI in range of 0 - 3: (1)
462 Free settling regime with constant FI of 2, that is developed at low concentration of 300 mg.L⁻¹;
463 (2) Flocculation regime with FI < 3, where flocculation happens at SSC of 300 - 2700 mg.L⁻¹;
464 (3) Hindered regime with FI of approximately 1 because of the appearance of brackish
465 water and high SSC of > 2.7 g.L⁻¹. Flocs reach higher volumetric concentration for lower
466 mass concentrations when flocculation is reinforced by differential settling (Gratiot et al.,
467 2017).



468 **Fig. 5.** Sediment properties in the Mekong Land to Ocean Continuum: (a) Variation of settling velocity with SSC measured directly with SCAF
 469 instrument and (b) Variation of the flocculation index with SSC.

470 **4. Discussion**

471 *4.1. Suspended sediment transport mechanisms along the Mekong*

472 As mentioned in Section 2.2.4, the transport regime of suspended sediment along the LMR
473 may be characterized through the non-dimensional Rouse number (R_o). For the upstream
474 fluvial environment, the computed shear velocities were similar in the different sections
475 monitored, $u_* = 0.03 \text{ m.s}^{-1}$ for the MK10 and $u_* = 0.04 \text{ m.s}^{-1}$ for MK16. The small difference
476 between the two cross-sections may be explained by the geometry of each cross-section,
477 MK10 cross-section being wider than MK16 cross-section. The shear velocity in the Tonle
478 Sap is 0.008 m.s^{-1} by using SLIM simulation obtained by Le et al. (submitted); while a value
479 of 0.010 m.s^{-1} is obtained by using the Inner law. The R_o values in the estuary are estimated
480 based on two representative particle sizes ($15 \mu\text{m}$ for fine particles and $300 \mu\text{m}$ for sand) and
481 the shear velocity is estimated with the recent work of Eidam et al. (2017).

482 The R_o values estimated for the fluvial, lacustrine and estuary environments are summarized
483 in Table 1. In the fluvial environment, the R_o ranges between 0.002 and 0.009 at the two
484 monitored river cross section (MK10 and MK16), which corresponds to the washload mode.
485 Hence particles are presumably transported over long distances, without any interaction with
486 the riverbed. Few sand particles are presents in the MK10 and MK16 cross section samples,
487 with R_o values of 0.75 - 4.6. Its means that the very fine sand particles are strongly sorted over
488 the water depth, leading to a low suspension mode. As for the coarser sand fraction of the
489 riverbed, the stream was not able to transport them in suspension.

490 While R_o values of Tonle Sap samples vary from 0.005 – 0.015, corresponding to flow modes
491 ranging from washload to strong suspension load (Vanoni et al., 1946 and Udo et al., 2011). It
492 is assumed that sediments are deposited near bed during one part of the year, and eroded
493 under wind-induced currents during another part of the year. According to Kummur (2008), the
494 net budget of sediment is almost in equilibrium between deposition and erosion.

495 In the estuary, the value of the R_o for the fine sediments ranges between 0.007 - 0.058, which
496 corresponds to strong suspension mode; while the values for sand vary from 2.4 to
497 approximately 12, which corresponds to the bedload mode and sedimentation dominated
498 regime (Gugliotta et al., 2019). This finding coincides with the recent study of Marchesiello et
499 al. (2019) showing that the Mekong sediments consist of a mixture (fine sediments and sands)

500 under effects of complex forces. Thus coastal muds are exposed to wave-induced
 501 resuspension and wind-induced transport, while sands are concentrated near the estuaries.

502 **Table 1.** Ro value in two different conditions

Sample	Mean Diameter (μm)	u_* (m.s^{-1})		w_s (m.s^{-1})		Rouse value	
		Law of Wall	Modelled results	SCAF	Stokes' Law	Min	Max
Fluvial (MK10)	19 ± 2	0.029	-	2.0E-05	1.2E-04	0.002	0.009
Fluvial (MK16)	18 ± 4	0.041	-	8.0E-05	1.2E-04	0.005	0.007
Tonle Sap	7 ± 2	0.014	0.008	5.0E-05	2.0E-05	0.005	0.015
Estuary fine sediment	15 ± 2	-	0.01	3.0E-05	2.4E-04	0.007	0.058
Estuary sand	300 ± 30	-	0.02	2.0E-02	9.5E-02	2.439	11.6

503 *4.2 Predominance of flocculi in the LMR and consequences for sediment transport*

504 As quantified in this paper, flocculi is the dominant particles population in all three
 505 environments monitored at regional scale (46 % in the fluvial environment, 78 % in the lake
 506 and 78 % in the estuary). The existence of sand was noticed, but can mostly be found near the
 507 bed with few percent of volume.

508 In the Lower Mekong River as in many other large hydrosystems under tropical climates, we
 509 may anticipate that particles' populations (and its consequences) fluctuate seasonally and year
 510 after year. As designed, this study cannot catch these variations, however, we believe that it
 511 describes a general pattern that could be helpful when establishing some monitoring strategies
 512 in similar large tropical hydrosystems in South East Asia, and probably elsewhere. At large
 513 scale, Rouse analysis presented in Table 1 showed that particles are mainly transported with a
 514 strong suspension regime, evenly as washload by river flow. By these modes, they are
 515 transported abundantly along the main river and tributaries, partially over the floodplains
 516 during the flood season (Kondolf et al., 2014, Manh et al., 2014, Manh et al., 2015) and then,
 517 are deposited along shore and on the whole subaqueous delta, before having cycles of
 518 resuspension/deposition, principally under waves forcing (Marchesiello et al., 2019). Our
 519 measurements in the fluvial section show that few sands are transported in the water column
 520 because their transport, which do not flocculate, is completely governed by the stream power.
 521 During high flow with enhanced stream powers working with other sediment sources
 522 (riverbanks and floodplains), the finest sands are lifted into upper layer.

523 This methodology can explain two distinct transport modes of two particles populations in the
524 Mekong estuary: washload is well mixed throughout the water column and sand are
525 transported prevailing near the bottom. It leads to distinct geomorphological forms, with the
526 presence of alternated tidal flats and sand bars as observed in many river mouths (Ta et al.,
527 2002; Gupta et al., 2002; Anthony, 2015).

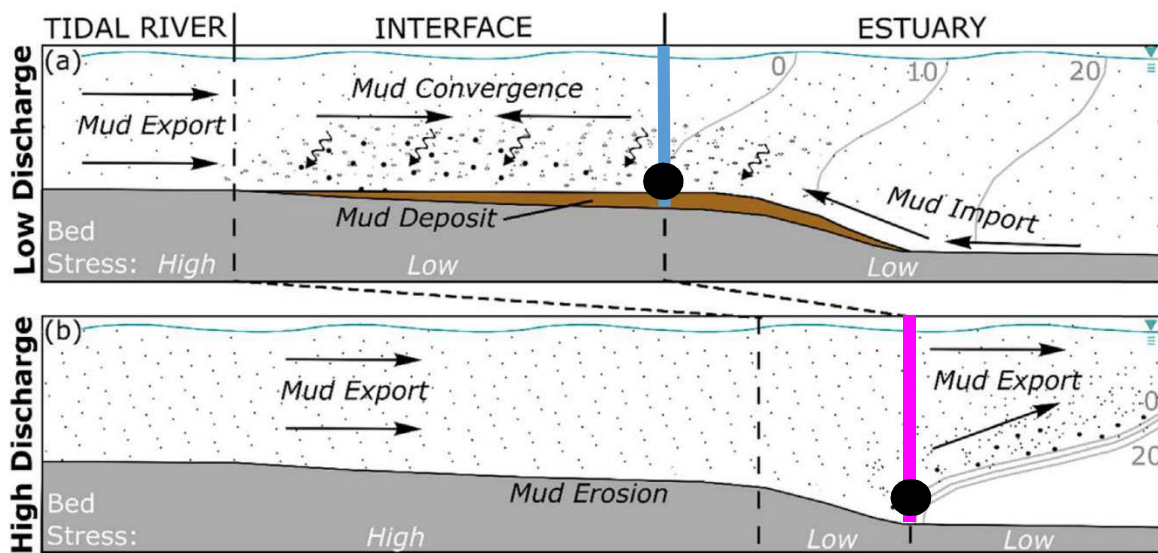
528 *4.3. Occurrence of fluid mud layers in the Mekong estuary*

529 According to measured data during our three surveys in the estuary, a fluid mud layer was
530 sometimes formed near bottom, with SSC values abruptly increasing beyond 0.4 g.L^{-1} ,
531 corresponding to the transition to the flocculation regime (Fig. 5; Gratiot et al., 2017). Fig. 6
532 sketches the sediment transport from the river to the estuary in low flow season (a) and high
533 flow season (b) with locations of vertical profile sampling. In this figure, the blue profile
534 represents a schematic profile measured in low flow season and the purple one represents a
535 profile measured in high flow season. Fig. 7 reports all SSC value observed near bottom ($z =$
536 $0.9h - SSC_{nb}$) for the vertical profiles realized in the estuary in December 2015 (50 profiles),
537 March 2016 (44 profiles) and October 2016 (47 profiles). Each vertical profile is represented
538 by a single point in Fig. 7. The three curves show the sorted distribution of all SSC_{nb} values
539 for the three seasons. The curves show that the percentage of profiles which exhibits high SSC
540 values, compatible with fluid mud layer occurrence, is very high during low flow season
541 (66 % of profiles in Dec 2015 and 95 % profiles in March 2016) and is much smaller during
542 high flow season (9 % profiles in October 2016).

543 By multiplying SSC_{nb} values with the corresponding settling velocity w_s reported in Fig. 5, we
544 can estimate the settling flux capacity of fluid mud layers $\phi = SSC_{nb} \times w_s$ and thus assess
545 their potential contribution to sedimentation (Fig. 7b). The cumulated sorted series
546 demonstrate the strong linearity between sediment concentration and settling flux (i.e.
547 potential of sedimentation). Fig.7c shows that the 10 % of the most concentrated fluid mud
548 layers contributes to 60 % of the sedimentation during low flow season (blue curves) and
549 more than 98 % during high flow season (purple curve).

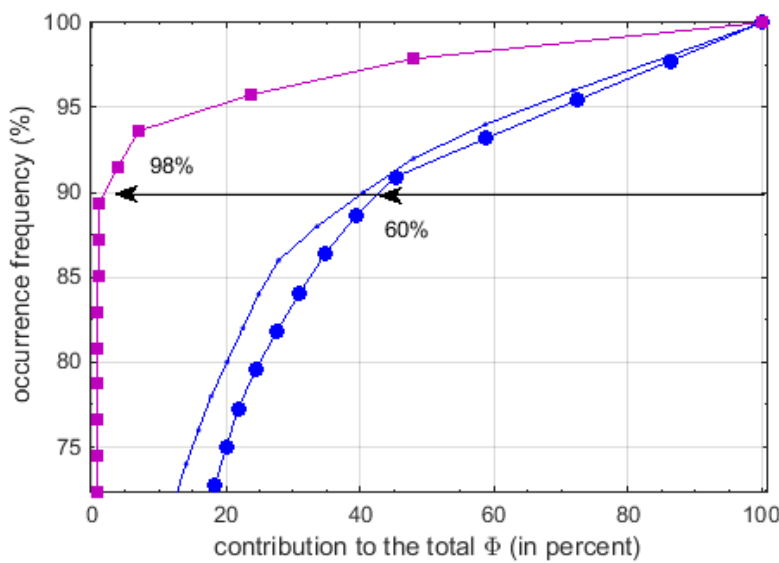
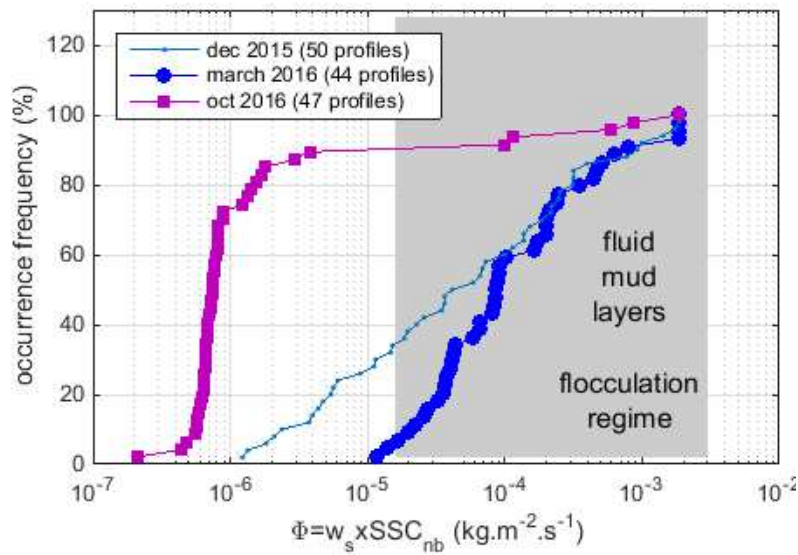
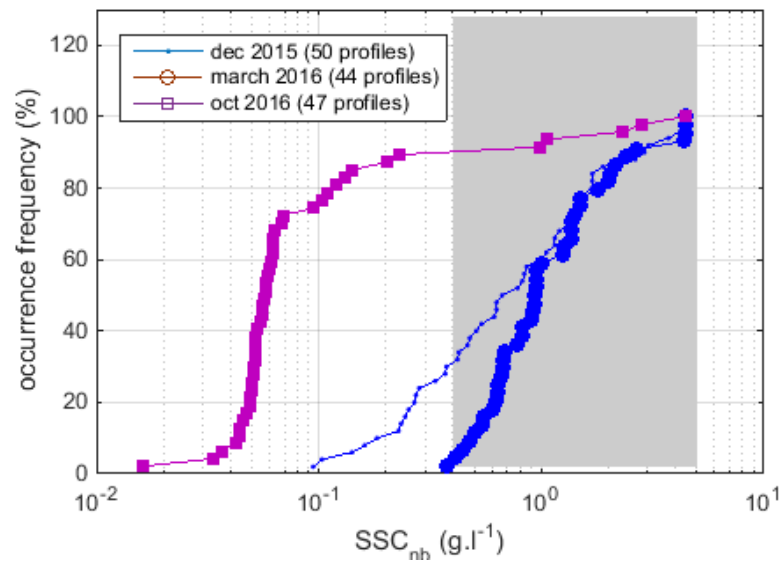
550 As a preliminary conclusion, our study confirms the existence of fluid mud layers and
551 quantifies broadly their frequency of occurrence in the estuary. Fluid mud layers are observed
552 within distances of approximately 30 km from the coastlines in both high flow and low flow
553 seasons. However according to Wolanski et al. (1998), the location of fluid mud layer in the

554 Mekong estuary varies spatially with river discharges and tides. In the high flow season, most
 555 of sediment deposits in shallow coastal waters, approximately 10 - 20 km from the coast
 556 (Wolanski et al., 1998 and Marchesiello et al., 2019). In low flow season, fine sediment is
 557 well mixed with saline water penetrating about 40 km inland, carrying sediment up-river to a
 558 turbidity maximum zone. Further upstream, at Can Tho, approximately 120 km from the
 559 coast, no turbidity maximum is found in the freshwater region of the estuary. Thus the
 560 positions of fluid mud layers and turbidity maximum, which are promoted by SSC
 561 concentration in the range $0.4 - 4 \text{ g.L}^{-1}$, can hardly be observed for distances higher than 120
 562 km inland. This situation could change in the future, under the cumulated effect of subsidence
 563 and sea level rise.



564
 565 **Fig 6.** Conceptual summary of salinity stratification (grey lines), SSC (dot concentration),
 566 relative near-bed shear stress, suspended particle aggregation (dot size), net sediment
 567 advection (black arrows), and mud deposition/erosion within the tidal river, tidal river –
 568 estuary interface, and estuary during (a) low and (b) high discharge seasons. Relative weight
 569 of transport arrows vary with season and regime. Not drawn to scale (after McLachlan et al.,
 570 2017). The blue line shows the vertical profile in low flow season and the purple line shows
 571 one in high flow season with SSC. The black dot shows the sampling height (near bottom, at
 572 0.9 h).

573 According to Spearman and Manning (2008), the mass balance between accretion and erosion
 574 of cohesive sediment during tidal cycles in estuarial location can occur when threshold shear
 575 stresses for both deposition and erosion operate simultaneously.



(a) **Fig 7.** Data corresponds to SSC measured near bottom (SSC_{nb}). Data are sorted from lowest to highest SSC (a), corresponding settling flux (b) and contribution to the total (c). The blue line shows the vertical profile in December 2015; the blue line with dots shows one in March 2016 and the purple line shows one in October 2016 with SSC near bed.

(c)

576 4.4. Implication for Mekong Delta management

577 In the MD, the flocculation process plays an essential role in the formation of fluid mud layer
578 by enhancing the downward flux of sediment when freshwater mixes with seawater and
579 sediments become trapped at the convergence point. Sediments leaving the MD appears to go
580 through cycles of trapping and resuspension in the estuary, before being partially advected
581 seaward on the subaqueous delta and alongshelf, where they are largely incorporated into
582 fluid mud along the bottom salinity front. The fluid muds have far-reaching effects on the
583 coasts by reducing boundary shear stresses, attenuating of waves over a soft muddy bottom,
584 affecting water-column /seabed exchanges, and serving as the agent of outward growth of the
585 subaqueous delta (Marchesiello et al., 2019). In addition, fluid mud layers can lead to rise in
586 fluid viscosity and density, and the reduction of bottom shear stresses can affect on the tidal
587 wave propagation (Gabioux et al., 2005). Thus without flocculation, the particles would be
588 carried directly offshore (Kineke et al., 1996). The appearance of fluid mud layer under
589 flocculation regime provides a mechanism for rapid and strong sedimentation in the estuaries
590 and lead to local siltation and mud accretion. Once deposited in the bed, fluid mud layers
591 contribute to bedform development and stability (Schindler et al., 2015). We should underline
592 that bedform consolidation and stability is hardly predictable, because it depends on both
593 physical and biological near bed processes (Parson et al., 2016) that evolve continuously for
594 sediment mixtures containing cohesive mud and biologically active substances such as
595 microorganisms, bacteria and microphytobenthos who form biofilms (Malarkey et al., 2015).

596 How can we anticipate the impact of human activities on sediment dynamics, flocculation and
597 fluid mud layer formation at regional scale? As reported in the recent publications of Schmitt
598 et al. (2017) and Thi Ha et al. (2018), human pressure, through sediment trapping and sand
599 mining, already leads to a significant decrease of SSC in the estuaries. Our study points out
600 that SSC is a determining factor affecting, first flocculation, and secondly, the formation of
601 fluid mud layers in the Mekong estuary. There is a critical treshold of around $SSC = 0.4 \text{ g.L}^{-1}$,
602 that can be seen as a tipping point for sediment processes. If the occurrence of SSC beyond
603 that point decreases, the deposition rate will strongly reduce (no linear effects), while the
604 erosion rate will probably increase because of a decrease of sediment quantity, and because of
605 the reduction of drag coefficient in the regions of fluid muds (Dyer et al., 2002a), which
606 enhances boundary shear stresses nearshore, coinciding with erosional areas in the Mekong
607 estuaries (Kineke et al., 1996). As fluid mud layers in the Mekong estuaries are a key factor to

608 promote flocculation and “boost” natural sedimentation, we do believe that some regular
609 monitoring programs should be realized. In terms of coastal management, a simple measure
610 that should be seriously considered is mangrove reforestation. Because of cohesiveness,
611 sediment particles transported out into mangrove forests during tidal inundation flocculate and
612 form larger flocs. Thus mangroves are not just passive colonisers of mud banks but they are
613 active in trapping suspended sediment, with positive feedback on shore protection (Furukawa
614 et al., 1997; Anthony and Gratiot, 2012; Gratiot and Anthony, 2016). This mechanism was
615 recently characterized through a deep geomorphological study conducted along the muddy
616 coast of the Guianas. In this environment, which is comparable to the Mekong shore, Brunier
617 et al. (2019) observed and quantified some exceptional rates of muddy shoreline retreat
618 following mangrove removal for field rice production. Apart from this mechanism, mangroves
619 play a role as a buffer between sea and land to prevent river sediment from re-entrainment to
620 the ocean at ebb tide (Furukawa and Wolanski, 1996).

621 **5. Conclusions**

622 Field surveys and laboratory analysis were performed at regional scale in the upper fluvial,
623 lacustrine and lower estuarine environments to provide a physically-based assessment of
624 sediment transport regimes, flocculation, and fluid mud layer dynamics along the Lower
625 Mekong River (LMR). The independent evaluation of particle size and settling velocity
626 provides a good assessment of particles behaviour, and allows characterizing the R_o number
627 and corresponding regimes in a robust way. Suspended sediments in fluvial and lacustrine
628 environments are predominantly flocculi (97 % and 100 % of total volume, respectively) and
629 primary particles, the modes are transported as washload or with a regime of strong
630 suspension. Some of these particles (primary particles and flocculi) probably experience
631 phases of deposition and resuspension, mostly in the adjacent floodplain, during their routing
632 through the Mekong basin, but we observed comparable sub distributions for fluvial,
633 lacustrine and even estuarine environments. This finding indicates that the primary particles
634 and flocculi populations very probably reach the estuary without any important physical
635 transformations (i.e. with similar PSD). In the estuary, the complex mixing between fluvial
636 and coastal waters and sediments offers optimal conditions of salinity, that leads to a higher
637 diversity of particles, with significant proportions of microflocs and macroflocs (25 % of total
638 volume), in the sand size range (diameter > 300 μm).

639 The original estimation of flocculation indexes with SCAF instrument allows defining clearly
640 the flocculation regime. This later is the most efficient for SSC in the range of 0.4 – 4 g.L⁻¹. In
641 fluvial, lacustrine and estuarine environments, flocculation regime develops for the same
642 range of SSC, beyond ~0.4 g.L⁻¹. Flocculation then becomes a key process, but its impacts on
643 particles populations differs with the different environments. In the Tonle Sap lake,
644 flocculation promotes the aggregation of colloids and primary particles on flocculi. In the
645 estuarine environment, flocculation leads to the formation of a new population of particles, the
646 micro-flocs. In the fluvial environment, the data were too scarce to draw a clear conclusion, as
647 freshly eroded aggregates could not be yet in equilibrium with river hydro-sedimentary
648 conditions.

649 As a consequence of these microscopic changes at scales of particles, our study confirms the
650 regular occurrence of fluid mud layers (55 - 60% of occurrence) near bottom in the Mekong
651 delta with distance of less than 120 km from the coastline, concentrated in 30 km in both high
652 - and low - flow seasons. Fluid mud layers, which are intrinsically linked with flocculation
653 processes, are early steps of landforms evolutions and participate to the geomorphology of the
654 Mekong Delta (MD). In the light of this study and considering the degree of vulnerability of
655 the delta to ongoing hydro-sedimentary changes, we may provide two recommendations:
656 Firstly, the continental sediment flux needs to be restored (or at least maintained) and human
657 driven subsidence needs to be controlled. Under those conditions, fluid mud layers should
658 remain a driver of river and coastal geomorphology, as it has been the case over the last
659 millennia. Secondly, the perception of mangrove should be reconsidered as reforestation is
660 probably the optimal manner, in both technical and environmental aspects, for ensuring
661 sediment trapping and preserving fluid mud layers and mudflat, with positive feedbacks on
662 mangrove colonization. In other words, mangroves cannot compensate regional
663 disequilibrium in sediment balance, but they can facilitate the transformation of diluted
664 suspended sediment into fluid mud layers.

665 Taking into account the degree of uncertainty of field and laboratory measurements with
666 natural fresh sediments, and the degree of variability of sediment properties in such large and
667 human-impacted systems, there is a clear interest to adopt a monitoring strategy that would
668 extend the study in time and space.

669

670 **Acknowledgements**

671 The authors would like to thank the Université catholique de Louvain, Belgium for Hoang-
672 Anh Le's doctoral fellowship, the Institut de Recherche pour le Développement (IRD -
673 France) to support the field surveys in Laos and in Vietnam with the financial support of
674 the Lower Mekong Delta coastal zones project (<http://lmdcz.siwrr.org.vn>). We also would like
675 to thanks VolTransMESKONG CNES/TOSCA project to support the monitoring in Cambodia
676 with the technical and scientific support of staff from LOG UMR8187 and the Institute of
677 Technology of Cambodia, especially.

678 **References**

- 679 1. Anthony, E. J., & Gratiot, N. (2012). Coastal engineering and large-scale mangrove
680 destruction in Guyana, South America: Averting an environmental catastrophe in the
681 making. *Ecological Engineering*, 47, 268-273.
- 682 2. Anthony, E.J., (2015). Wave influence in the construction, shaping and destruction of river
683 deltas: A review. *Marine Geology*, 361, 53-78.
- 684 3. Antoine, G., Cazilhac, M., Monnoyer, Q., Jodeau, M., Gratiot, N., Besnier, A. L., ... & Le
685 Brun, M. (2015, April). Lateral and vertical heterogeneity of flow and suspended sediment
686 characteristics during a dam flushing event, in high velocity conditions. In EGU General
687 Assembly Conference Abstracts (Vol. 17).
- 688 4. Azhikodan, G., & Yokoyama, K. (2018). Sediment transport and fluid mud layer formation
689 in the macro-tidal Chikugo river estuary during a fortnightly tidal cycle. *Estuarine, Coastal
690 and Shelf Science*, 202, 232-245.
- 691 5. Azrulhisham, E. A., & Azri, M. A. (2018, February). Application of LISST instrument for
692 suspended sediment and erosive wear prediction in run-of-river hydropower plants.
693 In 2018 IEEE International Conference on Industrial Technology (ICIT) (pp. 886-891).
694 IEEE.
- 695 6. Bachmann, R. W., Hoyer, M. V., Vinzon, S. B., & Daniel Jr, E. C. (2005). The origin of
696 the fluid mud layer in Lake Apopka, Florida. *Limnology and Oceanography*, 50(2), 629-
697 635.
- 698 7. Balica, S., Dinh, Q., Popescu, I., Vo, T. Q., & Pham, D. Q. (2014). Flood impact in the
699 Mekong delta, Vietnam. *Journal of Maps*, 10(2), 257-268.

- 700 8. Brunier, G., Anthony, E. J., Gratiot, N., & Gardel, A. (2019). Exceptional rates and
701 mechanisms of muddy shoreline retreat following mangrove removal. *Earth Surface*
702 *Processes and Landforms*.
- 703 9. Camenen, B., & van Bang, D. P. (2011). Modelling the settling of suspended sediments for
704 concentrations close to the gelling concentration. *Continental Shelf Research*, 31(10),
705 S106-S116.
- 706 10. Camenen, B., Le Coz, J., Dramais, G., Peteuil, C., Fretaud, T., Falgon, A., ... & Moore, S.
707 A. (2014). A simple physically-based model for predicting sand transport dynamics in the
708 Lower Mekong River. In *Proc. River Flow conference*, Lausanne, Switzerland, 8p.
- 709 11. Castro-Orgaz, O., Giráldez, J. V., Mateos, L., & Dey, S. (2012). Is the von Kármán
710 constant affected by sediment suspension?. *Journal of Geophysical Research: Earth*
711 *Surface*, 117(F4).
- 712 12. Comba, S., & Sethi, R. (2009). Stabilization of highly concentrated suspensions of iron
713 nanoparticles using shear-thinning gels of xanthan gum. *Water Research*, 43(15), 3717-
714 3726.
- 715 13. Darby, S. E., Hackney, C. R., Leyland, J., Kumm, M., Lauri, H., Parsons, D. R., ... &
716 Aalto, R. (2016). Fluvial sediment supply to a mega-delta reduced by shifting tropical-
717 cyclone activity. *Nature*, 539(7628), 276.
- 718 14. Droppo, I. G., Nackaerts, K., Walling, D. E., & Williams, N. (2005). Can flocs and water
719 stable soil aggregates be differentiated within fluvial systems?. *Catena*, 60(1), 1-18.
- 720 15. Dyer, K. R., Bale, A. J., Christie, M. C., Feates, N., Jones, S., & Manning, A. J. (2002).
721 The turbidity maximum in a mesotidal estuary, the Tamar Estuary, UK: I. Dynamics of
722 suspended sediment. In *Proceedings in Marine Science* (Vol. 5, pp. 203-218). Elsevier.
- 723 16. Dyer, K. R., Bale, A. J., Christie, M. C., Feates, N., Jones, S., & Manning, A. J. (2002b).
724 The turbidity maximum in a mesotidal estuary, the Tamar estuary, UK: II. The floc
725 properties. In *Proceedings in Marine Science* (Vol. 5, pp. 219-232). Elsevier.
- 726 17. Edmonds, D. A., & Slingerland, R. L. (2010). Significant effect of sediment cohesion on
727 delta morphology. *Nature Geoscience*, 3(2), 105.
- 728 18. Eidam, E. F., Nittrouer, C. A., Ogston, A. S., DeMaster, D. J., Liu, J. P., Nguyen, T. T., &
729 Nguyen, T. N. (2017). Dynamic controls on shallow clinoform geometry: Mekong Delta,
730 Vietnam. *Continental Shelf Research*, 147, 165-181.
- 731 19. Farrell, E. J., & Sherman, D. J. (2013). Estimates of the Schmidt Number for vertical flux
732 distributions of wind-blown sand. *Journal of Coastal Research*, 65(sp2), 1289-1295.

- 733 20. Fennessy, M. J., Dyer, K. R., & Huntley, D. A. (1994). Size and settling velocity
734 distributions of flocs in the Tamar Estuary during a tidal cycle. *Netherlands Journal of*
735 *Aquatic Ecology*, 28(3-4), 275-282.
- 736 21. Fettweis, M., Francken, F., Pison, V., & Van den Eynde, D. (2006). Suspended particulate
737 matter dynamics and aggregate sizes in a high turbidity area. *Marine Geology*, 235(1-4),
738 63-74.
- 739 22. Furukawa, K., & Wolanski, E. (1996). Sedimentation in mangrove forests. *Mangroves and*
740 *Salt Marshes*, 1(1), 3-10.
- 741 23. Furukawa, K., Wolanski, E., & Mueller, H. (1997). Currents and sediment transport in
742 mangrove forests. *Estuarine, Coastal and Shelf Science*, 44(3), 301-310.
- 743 24. Gabioux, M., Vinzon, S. B., & Paiva, A. M. (2005). Tidal propagation over fluid mud
744 layers on the Amazon shelf. *Continental Shelf Research*, 25(1), 113-125.
- 745 25. Gratiot, N., Gardel, A. and Anthony, E.J., 2007. Trade-wind waves and mud dynamics on
746 the French Guiana coast, South America: input from ERA-40 wave data and field
747 investigations. *Marine Geology*. 236, 15-26.
- 748 26. Gratiot, N., Coulaud, C., Legout, C., Mercier, B., Mora, H., & Wendling, V. (2015). Unit
749 for measuring the falling speed of particles in suspension in a fluid and device comprising
750 at least one measuring unit and one automatic sampler. Patent - Publication number
751 WO2015055963 A, 1.
- 752 27. Gratiot, N., & Anthony, E. J. (2016). Role of flocculation and settling processes in
753 development of the mangrove-colonized, Amazon-influenced mud-bank coast of South
754 America. *Marine Geology*, 373, 1-10.
- 755 28. Gratiot, N., Bildstein, A., Anh, T. T., Thoss, H., Denis, H., Michallet, H., & Apel, H.
756 (2017). Sediment flocculation in the Mekong River estuary, Vietnam, an important driver
757 of geomorphological changes. *Comptes Rendus Geoscience*, 349(6-7), 260-268.
- 758 29. Gugliotta, M., Saito, Y., Nguyen, V. L., Ta, T. K. O., & Tamura, T. (2019). Sediment
759 distribution and depositional processes along the fluvial to marine transition zone of the
760 Mekong River delta, Vietnam. *Sedimentology*, 66(1), 146-164.
- 761 30. Gupta, A., & Liew, S. C. (2007). The Mekong from satellite imagery: A quick look at a
762 large river. *Geomorphology*, 85(3-4), 259-274.
- 763 31. Hai, P. T., Masumoto, T., & Shimizu, K. (2008). Development of a two-dimensional finite
764 element model for inundation processes in the Tonle Sap and its environs. *Hydrological*
765 *Processes: An International Journal*, 22(9), 1329-1336.

- 766 32. Hung, N. N., Delgado, J. M., Güntner, A., Merz, B., Bárdossy, A., & Apel, H. (2014).
767 Sedimentation in the floodplains of the Mekong Delta, Vietnam Part II: deposition and
768 erosion. *Hydrological Processes*, 28(7), 3145-3160.
- 769 33. Kineke, G. C., Sternberg, R. W., Trowbridge, J. H., & Geyer, W. R. (1996). Fluid-mud
770 processes on the Amazon continental shelf. *Continental Shelf Research*, 16(5-6), 667-696.
- 771 34. Kondolf, G. M., Rubin, Z. K., & Minear, J. T. (2014). Dams on the Mekong: Cumulative
772 sediment starvation. *Water Resources Research*, 50(6), 5158-5169.
- 773 35. Kummu, M., & Sarkkula, J. (2008). Impact of the Mekong River flow alteration on the
774 Tonle Sap flood pulse. *AMBIO: AMBIO*, 37(3), 185-193.
- 775 36. Kummu M, Tes S, Yin S, Adamson P, Jozsa J, Koponen J, Richey J, Sarkkula J (2014)
776 Water balance analysis for the Tonle Sap Lake - floodplain system. *Hydrological*
777 *Processes* 28(4):1722-1733.
- 778 37. Le, H. A., Lambrechts, J., Ortled, S., Gratiot, N., Deleersnijder, E., Soares-Fraza, S.,
779 (2019). An implicit wetting - drying algorithm for the Discontinuous Galerkin method:
780 Application to the Tonle Sap, Mekong River Basin. *Environmental Fluid Mechanics* (in
781 submission).
- 782 38. Lee, B. J., Fettweis, M., Toorman, E., & Molz, F. J. (2012). Multimodality of a particle
783 size distribution of cohesive suspended particulate matters in a coastal zone. *Journal of*
784 *Geophysical Research: Oceans*, 117(C3).
- 785 39. Malarkey, J., Baas, J. H., Hope, J. A., Aspden, R. J., Parsons, D. R., Peakall, J., ... & Bass,
786 S. J. (2015). The pervasive role of biological cohesion in bedform development. *Nature*
787 *communications*, 6, 6257.
- 788 40. Manh, N.V., Dung, N.V., Hung, N.N., Merz, B., & Apel, H. (2014). Large-scale
789 quantification of suspended sediment transport and deposition in the Mekong
790 Delta. *Hydrology and Earth System Sciences Discussions*, 11(4).
- 791 41. Manh, N.V, Dung, N. V., Hung, N. N., Kummu, M., Merz, B., & Apel, H. (2015). Future
792 sediment dynamics in the Mekong Delta floodplains: Impacts of hydropower
793 development, climate change and sea level rise. *Global and Planetary Change*, 127, 22-33.
- 794 42. Manning, A. J., Friend, P. L., Prowse, N., & Amos, C. L. (2007). Estuarine mud
795 flocculation properties determined using an annular mini-flume and the LabSFLOC
796 system. *Continental Shelf Research*, 27(8), 1080-1095.
- 797 43. Manning, A. J., Baugh, J. V., Spearman, J. R., & Whitehouse, R. J. (2010). Flocculation
798 settling characteristics of mud: sand mixtures. *Ocean dynamics*, 60(2), 237-253.

- 799 44. Manning, A.J., Baugh, J.V., Soulsby, R.L., Spearman, J.R., Whitehouse, R.J.S., 2011a.
800 Cohesive sediment flocculation and the application to settling flux modelling (Chapter 5).
801 In: Ginsberg, Silvia Susana (Ed.), *Sediment Transport*. InTech, Vienna, ISBN: 978-953-
802 307-189-3, pp. 91–116.
- 803 45. Manning, A. J., Baugh, J. V., Spearman, J. R., Pidduck, E. L., & Whitehouse, R. J.
804 (2011b). The settling dynamics of flocculating mud-sand mixtures: Part 1—Empirical
805 algorithm development. *Ocean Dynamics*, 61(2-3), 311-350.
- 806 46. Marchesiello, P., Nguyen, N.M., Gratiot, N., Loisel, H., Anthony, E.J. and Nguyen, T.,
807 2019. Erosion of the coastal Mekong delta: Assessing natural against man induced
808 processes. *Continental Shelf Research*, 181, 72-89.
- 809 47. McAnally, W. H., Friedrichs, C., Hamilton, D., Hayter, E., Shrestha, P., Rodriguez, H., ...
810 & ASCE Task Committee on Management of Fluid Mud. (2007). Management of fluid
811 mud in estuaries, bays, and lakes. I: Present state of understanding on character and
812 behavior. *Journal of Hydraulic Engineering*, 133(1), 9-22.
- 813 48. McLachlan, R. L., Ogston, A. S., & Allison, M. A. (2017). Implications of tidally - varying
814 bed stress and intermittent estuarine stratification on fine-sediment dynamics through the
815 Mekong's tidal river to estuarine reach. *Continental Shelf Research*, 147, 27-37.
- 816 49. Mehta, A. J. (1991). Understanding fluid mud in a dynamic environment. *Geo-Marine*
817 *Letters*, 11(3-4), 113-118.
- 818 50. Mekong River Commission portal, available at <http://www.mrcmekong.org/>.
- 819 51. Mikkelsen, O. A., Hill, P. S., & Milligan, T. G. (2006). Single-grain, microfloc and
820 macrofloc volume variations observed with a LISST-100 and a digital floc
821 camera. *Journal of Sea Research*, 55(2), 87-102.
- 822 52. Milliman, J. D., & Meade, R. H. (1983). World-wide delivery of river sediment to the
823 oceans. *The Journal of Geology*, 91(1), 1-21.
- 824 53. Nguyen, T. T., Némery, J., Gratiot, N., Garnier, J., Strady, E., Tran, V. Q., ... & Aimé, J.
825 (2019). Phosphorus adsorption/desorption processes in the tropical Saigon River estuary
826 (Southern Vietnam) impacted by a megacity. *Estuarine, Coastal and Shelf Science*,
827 106321.
- 828 54. Nittrouer, C. A., DeMaster, D. J., Eidam, E. F., Nguyen, T. T., Liu, J. P., Ogston, A. S., &
829 Phung, P. V. (2017). The Mekong continental shelf: The primary sink for deltaic sediment
830 particles and their passengers. *Oceanography*, 30(3), 60-70.

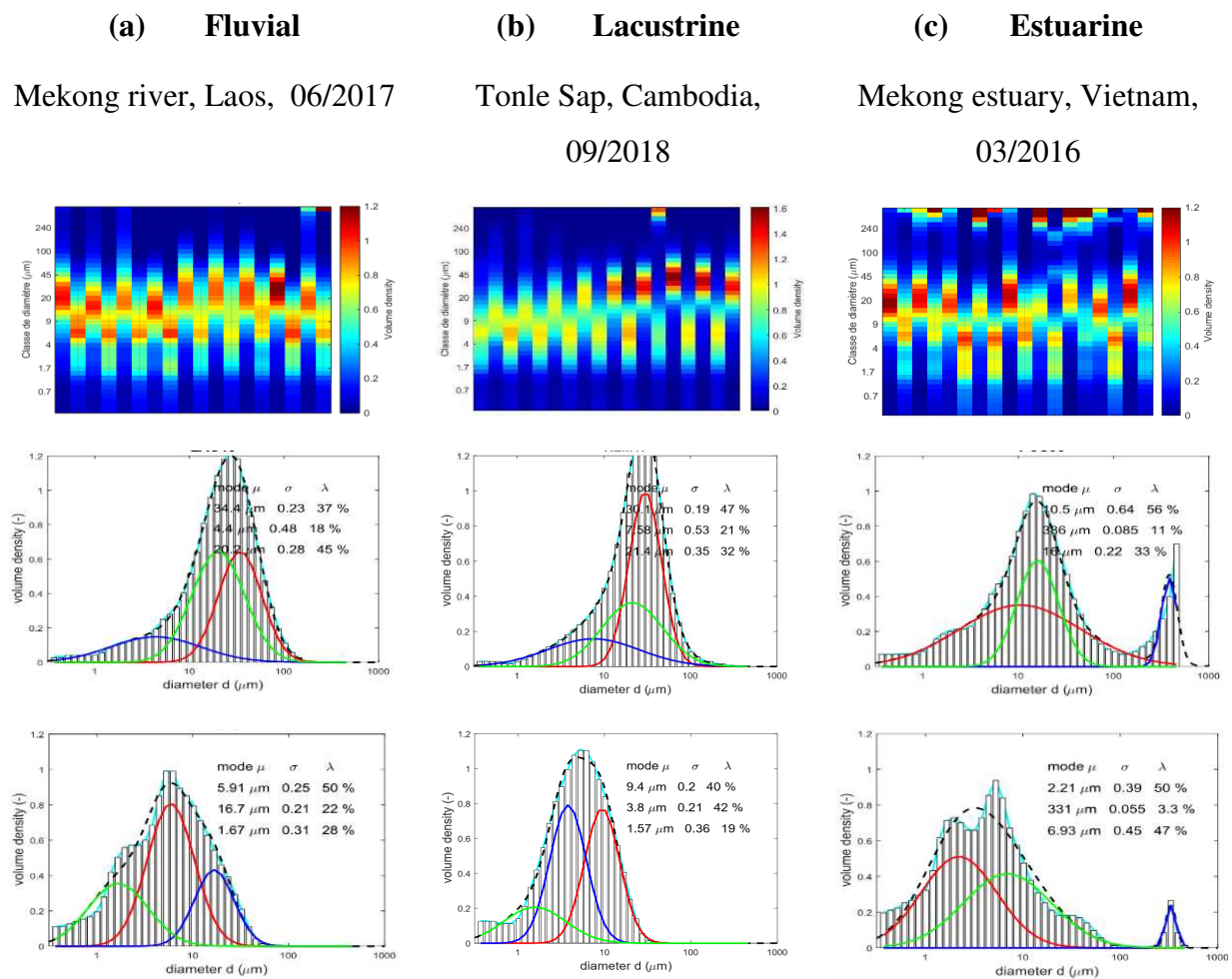
- 831 55. Nowacki, D. J., Ogston, A. S., Nittrouer, C. A., Fricke, A. T., & Van, P. D. T. (2015).
832 Sediment dynamics in the lower Mekong River: Transition from tidal river to
833 estuary. *Journal of Geophysical Research: Oceans*, 120(9), 6363-6383.
- 834 56. Parsons, D. R., Schindler, R. J., Hope, J. A., Malarkey, J., Baas, J. H., Peakall, J., ... &
835 Aspden, R. J. (2016). The role of biophysical cohesion on subaqueous bed form
836 size. *Geophysical research letters*, 43(4), 1566-1573.
- 837 57. Peteuil, C., Frétau, T., Wirz, C., Camenen, B., Guertault, L., Le Coz, J., & Dramais, G.
838 (2014). Importance of field observation for managing sediment fluxes in hydropower
839 projects design and operation. In *Proceedings of the 19th IAHR-APD Congress, Hanoi,*
840 *Vietnam.*
- 841 58. Ribolzi, O., Evrard, O., Huon, S., Rouw, A. De, Silvera, N., Latschack, O., Soulileuth, B.,
842 Lefèvre, I., Pierret, A., 2017. From shifting cultivation to teak plantation: effect on
843 overland flow and sediment yield in a montane tropical catchment. *Sci. Rep.* 1–12.
- 844 59. Rijn, L. C. V. (1984). Sediment transport, part II: suspended load transport. *Journal of*
845 *Hydraulic Engineering*, 110(11), 1613-1641.
- 846 60. Rouse, H. (1937). Modern conceptions of the mechanics of fluid turbulence. *Trans*
847 *ASCE*, 102, 463-505.
- 848 61. Santini, W., Camenen, B., Coz, J. L., Vauchel, P., Guyot, J. L., Lavado, W., ... & Espinoza
849 Villar, R. (2019). An index concentration method for suspended load monitoring in large
850 rivers of the Amazonian foreland. *Earth Surface Dynamics*, 7(2), 515-536.
- 851 62. Schindler, R. J., Parsons, D. R., Ye, L., Hope, J. A., Baas, J. H., Peakall, J., ... & Paterson,
852 D. M. (2015). Sticky stuff: Redefining bedform prediction in modern and ancient
853 environments. *Geology*, 43(5), 399-402.
- 854 63. Schmitt, R. J. P., Rubin, Z., & Kondolf, G. M. (2017). Losing ground-scenarios of land
855 loss as consequence of shifting sediment budgets in the Mekong
856 Delta. *Geomorphology*, 294, 58-69.
- 857 64. Schelske, C. L. (2006). Comment on the origin of the “fluid mud layer” in Lake Apopka,
858 Florida. *Limnology and Oceanography*, 51(5), 2472-2480.
- 859 65. Seah, K. C., Qasim, G. H., Hong, Y. S., Kim, E., Kim, K. T., & Han, S. (2017).
860 Assessment of colloidal copper speciation in the Mekong River Delta using diffusive
861 gradients in thin film techniques. *Estuarine, Coastal and Shelf Science*, 188, 109-115.
- 862 66. Sequioa. LISST-Portable|XR User's Manual Version 1.2 (2016).
- 863 67. Siev S, Paringit EC, Yoshimura C, Hul S (2016) Seasonal Changes in the Inundation Area
864 and Water Volume of the Tonle Sap River and Its Floodplain. *Hydrology* 3(4):33-45.

- 865 68. Sim, S. Y., Chan, D. C. H., Huang, T. F., Chai, W., Isaacson, T., Flood Jr, J. C., ... &
866 Orzen, M. (2007). U.S. Patent No. 7,272,613. Washington, DC: U.S. Patent and
867 Trademark Office.
- 868 69. Sime, L. C., Ferguson, R. I., & Church, M. (2007). Estimating shear stress from moving
869 boat acoustic Doppler velocity measurements in a large gravel bed river. *Water Resources*
870 *Research*, 43(3).
- 871 70. Smardon, R. (2009). Restoration of the Tram Chim National Wildlife Preserve, Vietnam.
872 *Sustaining the World's Wetlands*, 153–178.
- 873 71. Sottolichio, A., Hurther, D., Gratiot, N., Bretel, P., 2011. Acoustic turbulence
874 measurements of near-bed suspended sediment dynamics in highly turbid waters of a
875 macrotidal estuary. *Continental Shelf Research*, 31, S36-S49.
- 876 72. Spearman, J., & Manning, A. J. (2008). On the significance of mud transport algorithms
877 for the modelling of intertidal flats. In *Proceedings in Marine Science* (Vol. 9, pp. 411-
878 430). Elsevier.
- 879 73. Stokes, G. G. (1857). On the effect of wind on the intensity of sound. *Brit. Assoc.*
880 *Report*, 22.
- 881 74. Ta, T. K. O., Nguyen, V. L., Tateishi, M., Kobayashi, I., Tanabe, S., & Saito, Y. (2002).
882 Holocene delta evolution and sediment discharge of the Mekong River, southern
883 Vietnam. *Quaternary Science Reviews*, 21(16-17), 1807-1819.
- 884 75. Thi Ha, D., Ouillon, S., & Van Vinh, G. (2018). Water and suspended sediment budgets in
885 the lower Mekong from high-frequency measurements (2009–2016). *Water*, 10(7), 846.
- 886 76. Toorman, E.A., Anthony, E., Augustinus, P.G.E.F., Gardel, A., Gratiot, N., Homenauth,
887 O., Huybrechts, N., Monbaliu, J., Moseley, K., Naipal, S. 2018. Interaction of mangroves,
888 coastal hydrodynamics and morphodynamics along the coastal fringes of the Guianas.
889 *Coastal research library series*, Springer book, pp 429-473.
- 890 77. Tran, D. D., Van Halsema, G., Hellegers, P. J., Hoang, L. P., Tran, T. Q., Kummu, M., &
891 Ludwig, F. (2018). Assessing impacts of dike construction on the flood dynamics of the
892 Mekong Delta. *Hydrology and Earth System Sciences*, 22(3).
- 893 78. Tri, V. K. (2012). Hydrology and hydraulic infrastructure systems in the Mekong Delta,
894 Vietnam. In *The Mekong Delta System* (pp. 49-81). Springer, Dordrecht.
- 895 79. Udo, K., & Mano, A. (2011). Application of Rouse's Sediment Concentration Profile to
896 Aeolian Transport: Is the suspension system for sand transport in air the same as that in
897 water?. *Journal of Coastal Research*, 2079-2083.

- 898 80. Uncles, R. J., Stephens, J. A., & Law, D. J. (2006). Turbidity maximum in the macrotidal,
899 highly turbid Humber Estuary, UK: Floccs, fluid mud, stationary suspensions and tidal
900 bores. *Estuarine, Coastal and Shelf Science*, 67(1-2), 30-52.
- 901 81. Van, L. A., & Van Bang, D. P. (2013). Hindered settling of sand–mud floccs mixtures:
902 From model formulation to numerical validation. *Advances in Water Resources*, 53, 1-11.
- 903 82. Van Leussen, 1994. Estuarine macroflocs and their role in fine-grained sediment
904 transport. Ph.D. thesis, University of Utrecht, The Netherlands.
- 905 83. Vanoni, V. A. (1946). Transportation of suspended sediment by water. *Trans. of*
906 *ASCE*, 111, 67-102.
- 907 84. W.C. Rouse. U.S. Patent and Trademark Office (1938).
- 908 85. Wendling, V., Gratiot, N., Legout, C., Droppo, I. G., Coulaud, C., & Mercier, B. (2015).
909 Using an optical settling column to assess suspension characteristics within the free,
910 flocculation, and hindered settling regimes. *Journal of Soils and Sediments*, 15(9), 1991-
911 2003.
- 912 86. Windt, C., Ebrahimian, A., & Traver, R. Flow Characterization of Stormwater Runoff in
913 Philadelphia. In *World Environmental and Water Resources Congress 2017* (pp. 365-371).
- 914 87. Winterwerp, J. C. (2002). On the flocculation and settling velocity of estuarine
915 mud. *Continental Shelf Research*, 22(9), 1339-1360.
- 916 88. Winterwerp, J. C. (2011). Fine sediment transport by tidal asymmetry in the high-
917 concentrated Ems River: indications for a regime shift in response to channel
918 deepening. *Ocean Dynamics*, 61(2-3), 203-215.
- 919 89. Wolanski, E., Huan, N. N., Nhan, N. H., & Thuy, N. N. (1996). Fine-sediment dynamics in
920 the Mekong River estuary, Vietnam. *Estuarine, Coastal and Shelf Science*, 43(5), 565-582.
- 921 90. Wolanski, E., Nhan, N. H., & Spagnol, S. (1998). Sediment dynamics during low flow
922 conditions in the Mekong River estuary, Vietnam. *Journal of Coastal Research*, 472-482.
- 923 91. Xing, F., Meselhe, E. A., Allison, M. A., & Weathers III, H. D. (2017). Analysis and
924 numerical modeling of the flow and sand dynamics in the lower Song Hau channel,
925 Mekong Delta. *Continental Shelf Research*, 147, 62-77.

Appendix

927 Fig. a, b, c display the detailed PSD for some representative samples collected in fluvial,
 928 lacustrine and estuarine environments, respectively. For clarity purposes, only a limited (nine)
 929 number of samples are represented in the first panel row. The second row exhibits
 930 representative PSDs without sonication and the last row is for representative PSDs with
 931 sonication. After two minutes of sonication, all three environments show higher percentages
 932 of smallest constituents, namely primary particles. The mean size of samples taken in the
 933 fluvial and lacustrine parts is smaller than ones taken in the estuary, especially after
 934 sonication, a considerable constituent of primary particles is found in the upper parts. In
 935 addition, the particle size in Tonle Sap was smallest, with mean diameter of approximately 7
 936 μm and primary particles are predominance. In contrast, the graphs illustrate the large
 937 variation of particle sizes in the delta, predominantly in range of 10 - 386 μm before
 938 sonication and 2.21 - 331 μm after sonication. It is clear that sand appears in the Mekong
 939 estuary with percentage of 11 %; a median diameter of $> 300 \mu\text{m}$.



940 **Fig.** PSD of three representative samples in fluvial, lacustrine and estuarine environments